RSC Advances

PAPER

View Article Online
View Journal | View Issue

Cite this: *RSC Adv.*, 2025, **15**, 32477

Hydrazineyl-linked imidazole[1,2-*a*]pyrimidine-thiazole hybrids: design, synthesis, and *in vitro* biological evaluation studies

Dinesha P,[a] Shivakumar Naik,[a] Udayakumar D,*[a] Revanasiddappa B. C,[b] Venkatesh Ranjan[b] and Naveena S. Veeranagaiah[c]

Received 2nd July 2025
Accepted 27th August 2025

DOI: 10.1039/d5ra04692k

rsc.li/rsc-advances

This research work details the use of a molecular hybridization technique to create a library of four series of hydrazineyl-linked imidazo[1,2-*a*]pyrimidine-thiazole derivatives. The structure of one of the final products, **K2**, was validated using single-crystal X-ray diffraction. Twenty-six novel hybrid molecules (**K1–K26**) were synthesized and tested for activity against the *mycobacterium tuberculosis* H37Rv strain. Three compounds (**K1**, **K2**, and **K3**) demonstrated significant inhibitory efficacy, with a MIC value of 1.6 μg mL^{-1}. The target compounds also showed significant antibacterial activity against four bacterial strains, namely *S. aureus*, *E. coli*, *B. subtilis*, and *P. aeruginosa*. In cytotoxicity studies using VERO cells, the potent *anti*-TB compounds (**K1**, **K2**, and **K3**) showed non-toxic profiles. Furthermore, *in silico* ADME assessment results, molecular docking (against InhA and CYP121), and DFT studies revealed the active compounds' significant potential as scaffolds for novel antitubercular medicines.

Introduction

The bacteria *Mycobacterium tuberculosis* causes tuberculosis (TB). The infection primarily affects the oxygen-rich macrophages of the lungs. It spreads when a few airborne bacteria from a person with active pulmonary tuberculosis enter the alveoli of a new host.[1] WHO's report in 2024 indicated that an estimated 10.8 million individuals worldwide caught tuberculosis. The disease kills almost 1.25 million people, with 1.09 million being HIV-negative and 161 000 being HIV-positive.[2] The TB epidemic has recently become more severe as a result of the rise of multidrug-resistant (MDR-TB) and extensively drug-resistant (XDR-TB) strains.[3] Bedaquiline and delamanid treat MDR-TB, although they have severe side effects and resistance problems. Detecting XDR-TB takes weeks, resulting in low success rates (30–50%), particularly among HIV patients.[4,5] New tuberculosis medications are desperately needed to combat the outbreak. The medications should: (1) reduce treatment time, (2) target MDR and XDR strains, (3) lower the number of pills, (4) allow for less frequent dosage (*e.g.*, once weekly), and (5) be compatible with HIV drugs.[6] InhA is a *trans*-enoyl-acyl carrier protein (ACP) reductase that is required for fatty acid synthesis (FAS), specifically in the FAS II pathway and mycolic acid production.[7] According to recent studies, the majority of produced drugs target the mycobacterial cell wall, namely the mycolic acid biosynthesis pathway, which is similar to FAS systems I and II.[8,9] Another new *anti*-TB target is the CYP121 enzyme. It catalyzes an unusual C–C bond formation between two tyrosine residues in cyclodityrosine to produce mycocyclosin.[10]

Our current research is aimed at delivering new anti-mycobacterial drugs by combining imidazo[1,2-*a*]pyrimidines and thiazole derivatives *via* a hydrazineyl-linker. This approach connects two active pharmacophores into one scaffold for biological evaluation. A review of FDA-approved drugs shows that pyrimidine makes up about 16% of the top six-membered nitrogen rings. Thiazole is common among five-membered rings, mainly due to its presence in β-lactam antibiotics, which make up 67% of thiazole-based drugs.[11] Three pyrimidine-based derivatives are in clinical trials. These include TBA-7371, GSK 2556286, and SPR720. GSK-286 disrupts mycobacterial cholesterol metabolism and is in Phase I trials. TBA-7371 inhibits DprE1, a key enzyme for mycobacterial cell wall synthesis. SPR720 targets bacterial DNA gyrase (GyrB) and is in Phase II trials (Fig. 1).[12] Some recent report shows that molecules with hydrazineyl functionality also show good *anti*-TB activity.[13–15]

Some current literature studies prove that imidazo[1,2-*a*] pyrimidine, thiazole, and hydrazineyl derivatives have strong antitubercular efficacy. Panchani and Joshi *et al.* discovered a series of benzo[4,5]imidazo[1,2-*a*]pyrimidine derivatives. Compounds having electronegative substituents such as 4-chloro, 4-bromo, and 4-fluoro showed high efficacy against the *Mycobacterium* Tb H37Rv strain.[16] Reddyrajula and

[a]*Organic and Medicinal Chemistry Laboratory, Department of Chemistry, National Institute of Technology Karnataka, Surathkal-575025, Mangalore, Karnataka, India. E-mail: udayakumar@nitk.edu.in; udayaravi80@gmail.com*

[b]*Department of Pharmaceutical Chemistry, NGSM Institute of Pharmaceutical Sciences, Paneer, Deralakatte, Mangalore-575018, Karnataka, India*

[c]*Department of Chemistry, Central University of Karnataka, Kalaburagi-585 367, Karnataka, India*

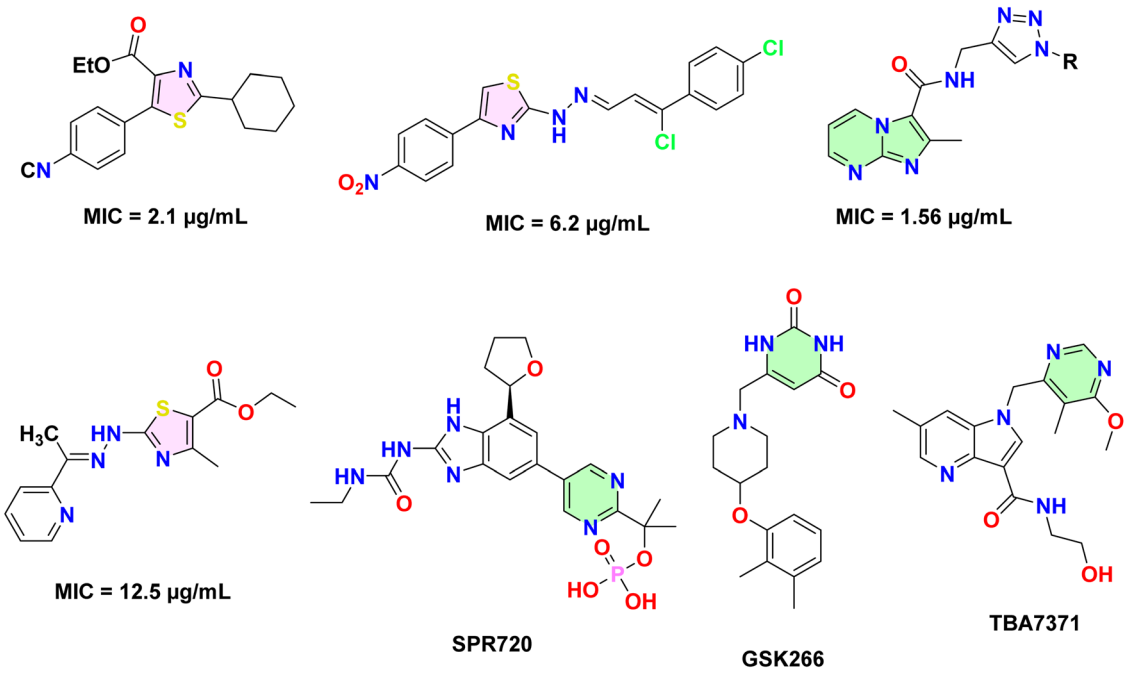

Fig. 1 Thiazole and pyrimidine-based *anti*-TB agents and pyrimidine-derived *anti*-TB compounds that are currently undergoing clinical trials.

Dalimba *et al.* developed a series of imidazo[1,2-*a*]pyrimidine-1,2,3-triazole derivatives. Compounds with methyl, methoxy, nitro, and cyano substituents showed significant activity, with a MIC of 1.56 μg mL^{-1}.[17] Roman *et al.* synthesized several thiazole-thiadiazole hybrid derivatives. Compound 1-(5-((6-bromopyridin-2-yl)amino)-1,3,4-thiadiazol-2-yl)-1-(4-methylthiazol-2-yl)ethanol showed high activity, with a MIC value of 1 μM.[18] Hublikar *et al.* developed a series of (*E*)-2-(2-allylidenehydrazinyl)thiazole derivatives. Compound 2-((*E*)-2-((*Z*)-3-chloro-3-(4-chlorophenyl)allylidene)hydrazinyl)-4-(4-nitrophenyl)thiazole shows strong inhibitory action with MIC 6.5 μg mL^{-1}.[19] Karale *et al.* reported the synthesis and *anti*-TB activity of 2,4,5-trisubstituted thiazole derivatives. The molecule ethyl 2-(4-cyanophenyl)-5-cyclohexylthiazole-4-carboxylate showed high activity against the H37Rv strain, with a MIC of 2.1 μg mL^{-1}, with 91% inhibition against dormant *M. tuberculosis* H37Ra and selectivity index (SI) of 35.8.[20] Makam *et al.* synthesized a series of 2-(2-hydrazinyl)thiazole derivatives. Among the two compounds, (*E*)-ethyl 4-methyl-(2-(1-(pyridin-2-yl)ethylidene)hydrazinyl)thiazole-5-carboxylate and (*E*)-ethyl 2-(2-(2-hydroxybenzylidene)hydrazinyl-4-methylthiazole-5-carboxylate, showed promising action against M.tb H37Rv, with MIC values of 12.5 and 25 μM, respectively.[21] We developed and synthesized four new series of hybrid compounds (**K1–K26**) that connected imidazo[1,2-*a*]pyrimidine and thiazole moieties into a single molecular structure, based on literature findings

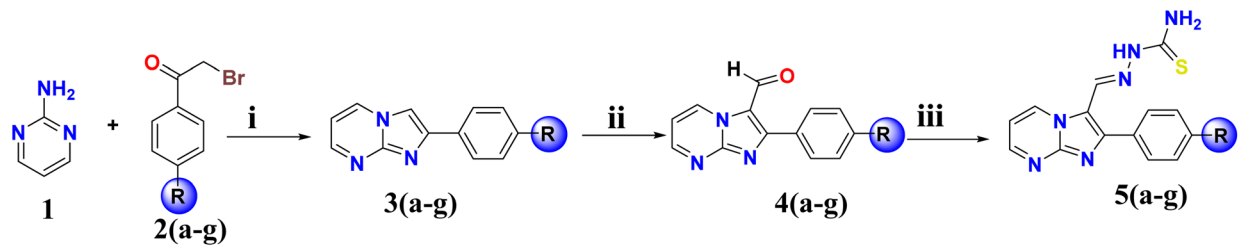

2a/ 3a/ 4a/ 5a, R = CH_3 **2e/ 3e/ 4e/ 5e, R = Br**

2b/ 3b/ 4b/ 5b, R = OCH_3 **2f/ 3f/ 4f/ 5f, R = CN**

2c/ 3c/ 4c/ 5c, R = F **2g/ 3g/ 4g/ 5g, R = H**

2d/ 3d/ 4d/ 5d, R = Cl

Scheme 1 Synthesis of intermediates: reagents and conditions: (i) acetone, reflux, 12 h (ii) $POCl_3$, DMF, reflux 2 h (iii) thiosemicarbazide, ethanol, conc. HCl reflux, 6 h.

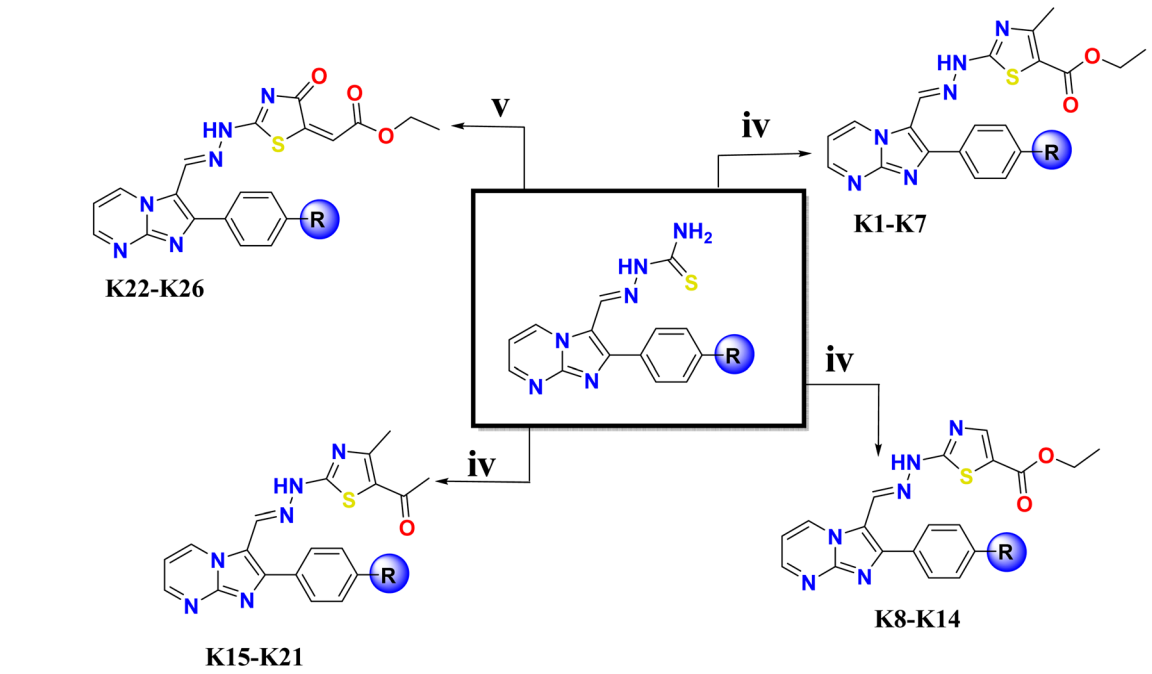

K1, K8, K15, K22, R = CH_3
K2, K9, K16, K23, R = OCH_3
K3, K10, K17, K24, R = F
K4, K11, K18, K25, R = Cl
K5, K12, K19, K26, R = Br
K6, K13, K20, R = CN
K7, K14, K21 R = H

Scheme 2 Synthesis of hydrazineyl linked imidazole[1,2-*a*]pyrimidine-thiazole derivatives (K1–K26): reagents and conditions: (iv) ethyl 2-chloro-3-oxobutanoate/ethyl 3-bromo-2-oxopropanoate/3-chloropentane-2,4-dione, glacial acetic acid, triethyl amine, methanol, reflux, 8 h (v) diethyl but-2-ynedioate, methanol, reflux, 6 h.

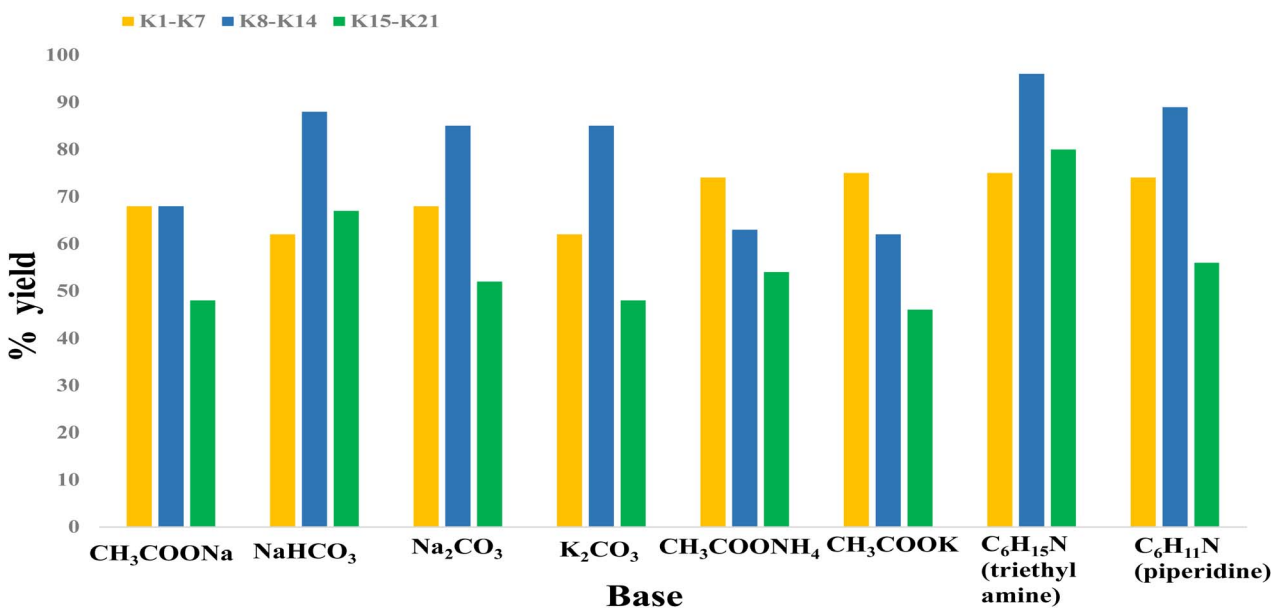

Fig. 2 Optimization of the synthetic route for compounds K1–K21, using different inorganic and organic bases.

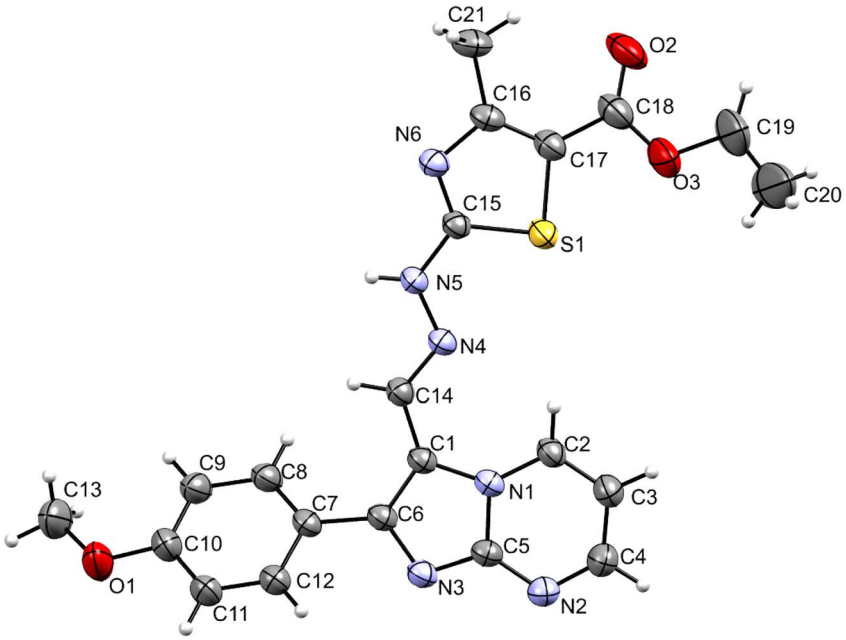

Fig. 3 ORTEP diagram showing the X-ray crystal structure of compound **K2**.

Table 1 Crystal data and structure refinement for **K2**

Identification code	**K2**	ρ_{calc} g cm^{-3}	1.309
Empirical formula	$C_{21}H_{20}N_6O_3S$	μ mm^{-1}	1.597
Formula weight	436.49	F (000)	3648.0
Temperature/K	299.00	Crystal size mm^{-3}	0.42 × 0.4 × 0.38
Crystal system	Tetragonal	Radiation	Cu Kα (λ = 1.54184)
Space group	$I4_1/a$	2θ range for data collection/°	6.4 to 148.58
a/Å	22.48035(17)	Index ranges	$-26 \le h \le 28$, $-27 \le k \le 12$, $-21 \le l \le 21$
b/Å	22.48035(17)	Reflections collected	21 613
c/Å	17.48441(18)	Independent reflections	4337 [R_{int} = 0.0245, R_{sigma} = 0.0174]
α/°	90	Data/restraints/parameters	4337/0/283
β/°	90	Goodness-of-fit on F^2	1.045
γ/°	90	Final R indexes [I> = 2σ (I)]	R_1 = 0.0452, wR_2 = 0.1402
Volume/Å^3	8836.03(16)	Final R indexes [all data]	R_1 = 0.0516, wR_2 = 0.1501
Z	16	Largest diff. Peak/hole per e Å^{-3}	0.32/−0.28

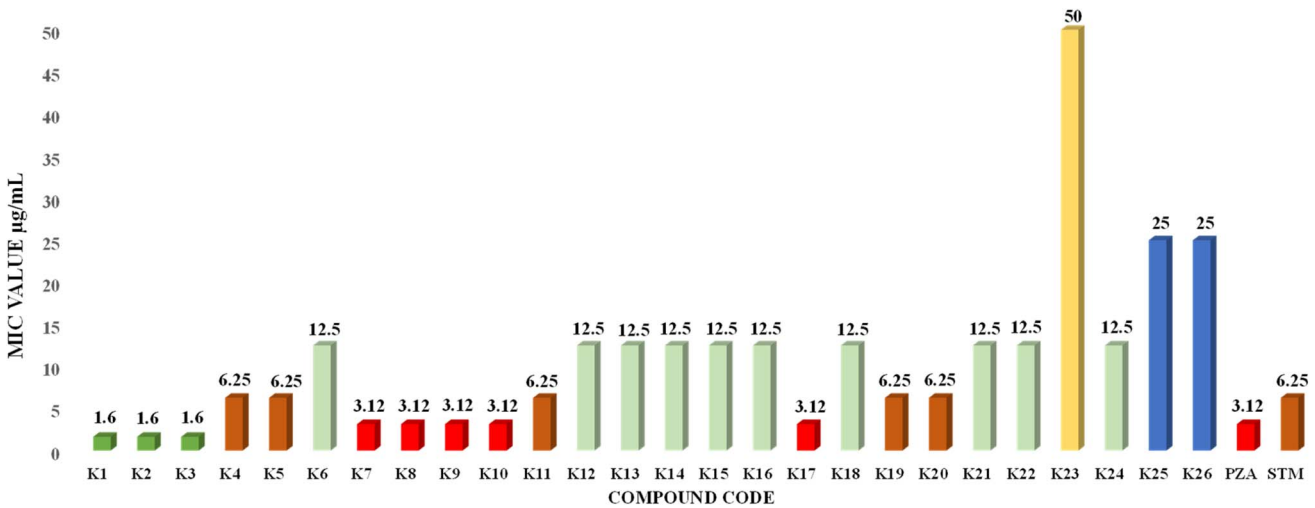

Fig. 4 Antitubercular efficacy of molecules **K1–K26** against *M. tuberculosis* H37Rv (PZA: pyrazinamide, and STM: streptomycin).

highlighting the promising antitubercular potential of pyrimidine and thiazole derivatives. This four-hybrid series of compounds contain a distinctive hydrazineyl functional group, which has the potential to improve the compound's capacity to interact with biological targets. Furthermore, inserting substituents at important functional sites, identified as R (Scheme 2), allows for structural refinement, increasing molecular diversity and modifying the biological activity of the molecules.

Results and discussion

Chemistry

The synthetic pathway of the imidazo[1,2-*a*]pyrimidine-thiazole hybrid derivatives (**K1–K26**) are illustrated in Scheme 1 and 2. In the first step, commercially available 2-aminopyrimidine (1) underwent a cyclization reaction with appropriately substituted phenacyl bromide derivatives **2(a–g)**, yielding substituted imidazo[1,2-*a*]pyrimidine derivatives **3(a–g)**. In the second step, substituted imidazo[1,2-*a*]pyrimidine carbaldehydes **4(a–g)** were obtained by reacting compounds (**3a–g**) with DMF and $POCl_3$ using Vilsmeier-Haack formylation. Compound (4) was condensed with thiosemicarbazide to get the intermediate **5(a–g)**. The final compounds, **K1–K21**, were obtained by cyclizing compound **5(a–g)** with ethyl 2-chloro-3-oxobutanoate/ethyl 3-bromo-2-oxopropanoate/3-chloropentane-2,4-dione in the presence of a base, glacial acetic acid as a catalyst, and absolute ethanol as a solvent. In the final step, we optimized the reaction conditions using various inorganic and organic bases. Reactions catalyzed by organic bases consistently gave significantly better yields compared to those catalyzed by inorganic bases. Among them, the reaction catalyzed by triethylamine provided the highest yield (Fig. 2). Compounds **K22–K26** were produced by cyclizing compound (5) with diethyl but-2-ynedioate using methanol as the solvent. The intermediate and target compounds (**K1–K26**) were validated using ^{1}H NMR, ^{13}C NMR, and mass spectrometry. The ^{1}H NMR spectrum of the intermediate compound (3) shows a peak at ~δ 8.6 ppm, confirming the imidazo[1,2-*a*] ring was successfully formed through cyclization. Compound 4's ^{1}H NMR spectrum shows a singlet peak at ~δ 10.09 ppm, confirming the formation of the formyl (–CHO) group. The singlet peak at ~δ 11.40 ppm indicates the

Table 2 The MIC values of target molecules (K1–K26)

Compound code	Structure of targeted compound	R	Mol wt	MIC (μg mL^{-1})	MIC μM
K1	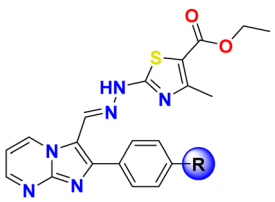	CH_3	420.1368	1.6	3.80
K2		OCH_3	436.1318	1.6	3.66
K3		F	424.1118	1.6	3.77
K4		Cl	440.0822	6.25	14.20
K5		Br	484.0317	6.25	12.91
K6		CN	431.1164	12.5	28.99
K7		H	406.1212	3.12	7.68
K8	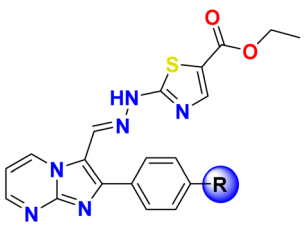	CH_3	406.1212	3.12	7.68
K9		OCH_3	422.1161	3.12	7.39
K10		F	410.0961	3.12	7.60
K11		Cl	426.0666	6.25	14.66
K12		Br	470.0161	12.5	26.59
K13		CN	417.1008	12.5	29.96
K14		H	392.1055	12.5	31.87
K15	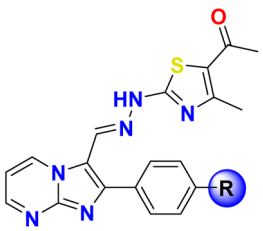	CH_3	390.1263	12.5	32.04
K16		OCH_3	406.1212	12.5	30.77
K17		F	394.1012	3.12	7.91
K18		Cl	410.0717	12.5	30.48
K19		Br	454.0211	6.25	13.76
K20		CN	401.1059	6.25	15.58
K21		H	376.1106	12.5	33.23
K22	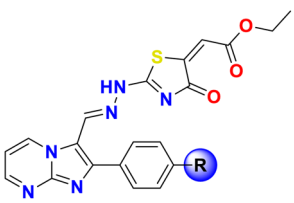	CH_3	434.1161	12.5	28.79
K23		OCH_3	450.1110	50	111.08
K24		F	438.0910	12.5	28.53
K25		Cl	454.0615	25	55.05
K26		Br	498.0110	25	50.19
PZA			123.1127	3.12	25.34
STM			581.5741	6.25	10.74

presence of the NH proton, while the peak at ~δ 8.70 ppm indicates the imine (CH=N) protons of the intermediate (6). The ^{1}H NMR spectrum of the final compounds **K1–K7** shows a singlet peak at ~δ 12.30 ppm representing the NH proton, and another peak at ~δ 8.5 ppm confirming the imine (CH=N) proton. Additionally, in the aliphatic region quartet and triplet peaks at ~δ 4.20 and 1.28 ppm represent the CH_2 and CH_3 groups, respectively. The compounds **K8–K14** were validated by ^{1}H NMR, with a signal at ~δ 12.29 ppm representing the NH proton. A quartet at ~δ 4.2 ppm and a triplet at ~δ 1.32 ppm were found to represent the CH_2 and CH_3 groups, respectively. In the ^{1}H NMR of the compounds **K15–K21**, a broad peak at ~δ 12.41 ppm confirms the presence of the NH proton, while a singlet at ~δ 8.60 ppm corresponds to the imine proton. In addition, two singlet peaks at ~δ 2.48 and ~δ 2.42 ppm indicate the two methyl groups. The final compounds **K22–K26** were structurally validated using ^{1}H NMR spectroscopy, with a characteristic peak at ~δ 12.95 ppm confirming the existence of the NH proton. Furthermore, a singlet at δ ~6.68 ppm corresponds to the alkene protons (HC=C). The ^{13}C NMR spectrum of the final compounds **K1–K14** shows a characteristic peak at ~δ 168 ppm, corresponding to the ester carbonyl carbon. Peaks at ~δ 60 and ~δ 14 ppm correspond to OCH_2 and CH_3 carbons, respectively. The compounds **K15–K21** show a distinct peak at ~δ 189 ppm, corresponding to the carbonyl carbon, and peaks at ~δ 29 and ~δ 19 ppm representing CH_3 carbon attached to the carbonyl group and CH_3 carbon attached to the thiazole ring respectively. The ^{13}C NMR spectra of compounds **K22–K26** show a peak at ~δ 168 ppm, indicating the ester carbonyl carbon and a peak at ~δ 111 ppm represents the alkene carbon (C=C). Single crystals of compound **K2** were produced by dissolving it in methanol and gently evaporating the solvent at room temperature. Crystals with dimensions of 0.2 × 0.19 × 0.17 mm^3 were created after 8–10 days. The molecular structure of **K2** was unequivocally validated by single-crystal X-ray diffraction (SC-XRD) analysis, as shown in (Fig. 3 and Table 1).

Biological studies

Anti-tubercular activity. The synthesized four series of hydrazineyl-linked imidazo[1,2-*a*]pyrimidine – thiazole hybrids (**K1–K26**) were tested for activity against the *M. tuberculosis* H37Rv strain (ATCC 27294) using the MABA method. Fig. 4 illustrates the MIC values (in μg mL^{-1}) for compounds **K1–K26** and standard drugs for comparison. The tested compounds had MIC values ranging from 1.6 to 50 μg mL^{-1}. Among the 26 target compounds, the first series **K1–K7** exhibited strong *anti*-TB

Table 3 Antibacterial activity (zone of inhibition in mm) of the compounds (K1–K26)[a]

	Zone of inhibition in mm			
	Gram positive bacteria		Gram negative bacteria	
Compound code	*S. aureus* (ATCC 23235)	*B. subtilis* (ATCC 6051)	*E. coli* (ATCC 25922)	*P. aeruginosa* (ATCC 27853)
K1	15	12	18	21
K2	15	15	18	18
K3	17	13	20	11
K4	13	14	20	11
K5	11	13	14	13
K6	17	14	10	15
K7	13	12	13	—
K8	12	—	17	19
K9	—	12	15	16
K10	12	16	15	12
K11	12	11	13	12
K12	15	10	14	12
K13	16	15	—	15
K14	15	14	12	15
K15	12	13	15	14
K16	18	—	—	11
K17	20	14	—	11
K18	18	15	15	12
K19	12	12	—	20
K20	17	15	14	12
K21	19	13	14	14
K22	15	15	24	13
K23	16	11	24	18
K24	10	—	10	11
K25	21	20	21	20
K26	15	15	—	—
Ciprofloxacin	36	30	35	30

[a] — No activity.

Table 4 MIC values, IC_{50}, and SI values of active compounds[a]

SI no	Compound code	MIC (μM) *	IC_{50} (μM)	SI
1	**K1**	3.80	183.03	48.16
2	**K2**	3.66	153.01	41.80
3	**K3**	3.77	161.75	42.90

[a] IC_{50}: concentration of the compound corresponding to 50% inhibition of the VERO cell lines. SI = IC_{50} against Vero cells/*MIC against *M. tuberculosis* H37Rv.

activity (Table 2). The compounds containing CH_3, OCH_3, and F substituents (**K1**, **K2**, **K3**) are the most effective inhibitors, with a MIC value of 1.6 μg mL^{-1}, surpassing the activity of all other molecules. The MIC values of the compound with unsubstituted Ph ring (**K7**) show a comparable activity with a MIC value of 3.12 μg mL^{-1}. Compounds with Cl and Br substituents, on the other hand, keep their MIC values at 6.25 μg mL^{-1}. In the second series of compounds (**K8–K14**), molecules with CH_3, OCH_3, and F (**K8**, **K9**, and **K10** respectively) substitutions show substantial activity, with a MIC value of 3.12 μg mL^{-1}. The other compounds with Br, CN, and H (unsubstituted phenyl ring) substituted (**K12**, **K13**, and **K14** respectively) maintain constant MIC values of 12.5 μg mL^{-1} regardless of substituents. In the third series of compounds (**K15–K21**), the F-substituted compound (**K17**) showed good inhibition with MIC 3.12 μg mL^{-1} whereas molecules with Br and CN substitutions displayed a MIC of 6.25 μg mL^{-1}. Four compounds substituted with CH_3, OCH_3, Cl, and H group (**K15**, **K16**, **K18**, **K21**) have maintained similar MIC values of 12.5 μg mL^{-1}. Compounds of the fourth series (**K23–K26**) are moderately active. The compounds substituted with CH_3/F (K22/K24) maintained a constant MIC value of 12.5 μg mL^{-1}. The Cl and Br substituted compounds showed MIC of 25 μg mL^{-1}. Among these four series of compounds, the first series of compounds (**K1–K7**) exhibited superior activity as compared to other series of compounds. Further, the F-substituted compounds (**K3**, **K10**, **K7**, and **K24**) in each of the four sets displayed the highest activity as compared to compounds substituted with other groups. The order of activity with halogen-substituted compounds is F > Br > Cl.

Antibacterial activity studies

The final compounds (**K1–K26**) were evaluated for antibacterial activity against four bacterial strains, *Staphylococcus aureus* (*S. aureus*), *Bacillus subtilis* (*B. subtilis*), *Pseudomonas aeruginosa* (*P. aeruginosa*), and *Escherichia coli* (*E. coli*) at a concentration of 100 μg mL^{-1}. The diffusion method was used to test the zones of inhibition, measured in mm. Ciprofloxacin was employed as the standard reference drug. Table 3 illustrates the results, including the zone of inhibition values for the reference drug and all the final compounds. The majority of the tested compounds had considerable antibacterial activity. In particular, compounds **K21**, **K17**, and **K25** showed high activity against *S. aureus*, with inhibition zones measuring 19, 20, and 21 mm, respectively. Compounds **K2**, **K13**, **K18**, **K20**, **K22**, **K10**, and **K25** showed moderate to good efficacy against *B. subtilis*, with inhibition zones measuring in the range of 15–20 mm. Compounds **K22**, **K23**, and **K25** had high antibacterial activity against *E. coli*, with zones of inhibition of 24, 24, and 21 mm respectively. Compounds **K1**, **K19**, and **K25** showed good action against *P. aeruginosa*, with inhibition zones measuring 21, 20, and 20 mm respectively. Overall, compound **K25** is more potent than the other compounds in terms of effectiveness against all four bacteria strains, with a zone of inhibition for all four bacterial strains above 20 mm.

Cytotoxicity. Compounds that showed potent antitubercular activity (MIC = 1.6 μg mL^{-1}) were tested for cytotoxicity in Vero cell lines generated from monkey kidney tissue using the MTT

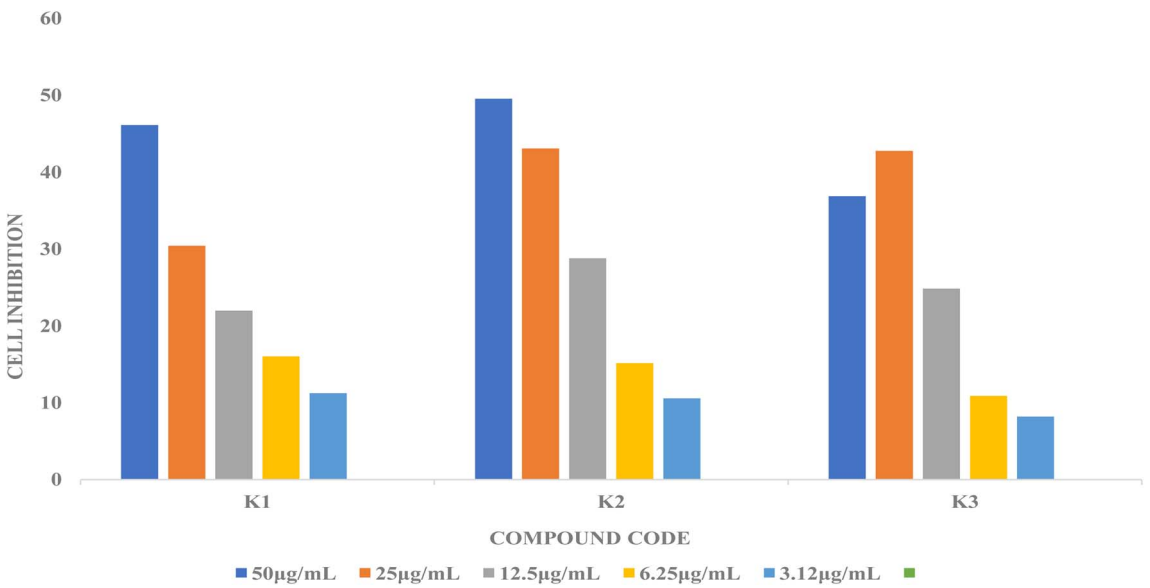

Fig. 5 The graphical representation of the cell viability of active compounds against Vero cells.

Table 5 ADME and physico–chemical parameters of the target compounds (K1–K26)[a]

Compound code	MW (≤500 Da)	HBD (≤5)	HBA (≤10)	QP log *P*(o/w) (≤5)	QP log *S* (≤0.5)	nRB (0–15)	PSA (≤140 Å)	QPPCaco (<25 nm s^{-1} is low; >500 nm s^{-1} is high	QP log Khsa (−1.5to1)	QP log BB (−3.0 to 1.2)	%OA (>80% is high:<25% is low
K1	420.1368	1	8.5	3.779	−6.565	6	97.872	602.262	0.302	−1.219	100
K2	436.1318	1	9.25	3.557	−6.205	7	106.077	601.883	0.143	−1.277	100
K3	424.1118	1	8.5	3.706	−6.36	6	97.869	603.111	0.188	−1.079	100
K4	440.0822	1	8.5	3.967	−6.745	6	97.876	603.415	0.262	−1.036	100
K5	484.0317	1	8.5	4.043	−6.858	6	97.876	603.311	0.285	−1.028	100
K6	431.1164	1	10	2.693	−6.916	7	123.696	124.79	−0.046	−2.155	80.23
K7	406.1212	1	8.5	3.473	−5.999	6	97.887	603.328	0.147	−1.183	100
K8	406.1212	1	8.5	3.373	−6.085	6	100.652	419.257	0.158	−1.373	93.63
K9	422.1161	1	9.25	3.149	−5.712	7	108.786	420.356	−0.001	−1.427	92.34
K10	410.0961	1	8.5	3.302	−5.883	6	100.632	419.711	0.045	−1.23	93.22
K11	426.0666	1	8.5	3.557	−6.254	6	100.633	419.37	0.117	−1.189	94.71
K12	470.0161	1	8.5	3.633	−6.366	6	100.636	419.435	0.139	−1.181	95.15
K13	417.1008	1	10	2.287	−6.431	7	126.44	87.014	−0.189	−2.293	75.05
K14	392.1055	1	8.5	3.196	−6.174	6	100.641	294.45	0.087	−1.632	89.85
K15	390.1263	1	8.5	3.121	−5.546	5	90.88	659.492	0.07	−1.028	95.67
K16	406.1212	1	9.25	2.904	−5.194	6	90.04	659.103	−0.086	−1.087	94.401
K17	394.1012	1	8.5	3.05	−5.346	5	90.856	660.332	−0.042	−0.888	95.27
K18	410.0717	1	8.5	3.305	−5.714	5	90.85	660.625	0.029	−0.844	96.76
K19	454.0211	1	8.5	3.38	−5.825	5	90.859	660.056	0.051	−0.836	100
K20	401.1059	2	10	2.039	−5.903	6	116.67	200.326	−0.273	−1.908	77.122
K21	376.1106	1	8.5	2.818	−4.988	5	90.867	660.037	−0.081	−0.993	93.09
K22	434.1161	1	10.5	2.641	−5.838	7	126.601	179.117	−0.137	−1.952	82.73
K23	450.1110	1	11.25	2.416	−5.466	8	134.855	179.189	−0.298	−2.007	81.42
K24	438.0910	1	10.5	2.571	−5.639	7	126.546	179.444	−0.248	−1.802	82.34
K25	454.0615	1	10.5	2.826	−6.001	7	126.546	180.228	−0.178	−1.76	83.867
K26	498.0110	1	10.5	2.901	−6.119	7	126.559	179.283	−0.156	−1.76	84.265

[a] MW: molecular weight, HBD: number of hydrogen bond donors, HBA: number of hydrogen bond acceptors, QP log *P* (o/w): logarithm of partition coefficient between *n*-octanol and water, QP log *S*: aqua solubility parameter, nRB: number of rotatable bonds, PSA: polar surface area, QPPCaco: Caco-2 cell permeability, QP log Khsa: Human serum albumin binding co-efficient, QP log BB: blood/brain partition co-efficient, %OA: percentage of oral absorption.

assay (3-(4,5-dimethylthiazol-2-yl)-2,5-diphenyltetrazolium bromide). The compounds' selectivity index (SI), IC_{50} values, and MIC values in μM are listed in Table 4. Fig. 5 depicts cell inhibition by active substances at different concentrations (3.125, 6.25, 12.5, 25, 50, 75, and 100 μg mL^{-1}). All of the active substances in the study showed less toxicity, with IC_{50} values ranging from 172.76 to 183.03 μM.

Computational studies

***In silico* ADME studies.** The ADME analysis of newly synthesized imidazo[1,2-*a*]pyrimidine-thiazole derivatives (**K1–K26**) was carried out employing the QikProp module to determine their pharmacokinetic and physicochemical features. According to a statistical study of regulatory agency databases, approximately 37% of pharmacological compounds do not continue in human clinical trials due to poor pharmacokinetic features, such as absorption, distribution, metabolism, and excretion (ADME).[22] Pharmacokinetic parameters of the final drugs (**K1–K26**) are summarizes Table 5. These parameters include molecular weight (Mol. Wt), partition coefficient (QP log Po/w), the number of hydrogen bond donors (HB) and acceptors (HA), polar surface area (PSA), blood–brain partition coefficient (QP log BB), human oral absorption (% HOA), binding to human serum albumin (QP log khsa), aqueous solubility (QP log *S*), and permeability across Caco-2 cells. To predict the oral bioavailability of drug molecules, employ the Lipinski rule of five (RO5). A compound with good oral bioavailability must meet specific criteria: a molecular weight less than (MW) of 500 g mol^{-1}, a partition coefficient (C log *P*) of no more than five, no more than five hydrogen bond donors (HBD) such as NH and OH groups, and no more than ten hydrogen bond acceptors (HBA), including O and N atoms.[23] Lipinski's rule of five analysis results revealed that all compounds (**K1–K26**) perfectly adhered to good oral bioavailability. PSA, which represents the surface area of nitrogen, oxygen, and bonded hydrogens, predicts hydrogen bonding and polarity. It is useful to analyze drug absorption, bioavailability, and tissue penetration. All the targeted molecules **K1–K26** had PSA values between 90.04 to 134.85 $Å^2$, indicating high oral bioavailability. The target compounds have a satisfactory water solubility (−4.898 to −6.916), which is a key component for assessing intestinal absorption in drug compounds (QP log $S \leq$ 0.5). The blood/brain partition coefficient (QP log BB) values are within the acceptable range of −2.155 to −0.836, confirming the compounds' ability to pass the blood–brain barrier. Another relevant measure is the human serum albumin binding coefficient (QP log Khsa), which has estimated values ranging from −0.298 to 0.302. As demonstrated, the percentage of human oral absorption for the first series of compounds (**K1–K7**) except for one molecule (**K6**) is 100%. Overall, all the compounds show more the 80% oral absorption.

Molecular docking studies. Molecular docking studies tend to be employed to investigate the binding interactions between ligands and a protein's active site, thereby estimating binding energy and confirming the molecular mechanisms involved. To investigate the binding approach of imidazo[1,2-*a*]pyrimidine – thiazole hybrids, all synthesized compounds (**K1–K26**) were subjected to molecular docking experiments against two target enzymes, enoyl-acyl carrier protein reductase (InhA) protein (PDB ID: 1P44) with co-crystal ligand GEQ and cytochrome P450 monooxygenase (CYP121) protein (PDB ID: 4KTF) with co-crystal ligand 1 TM. To ensure the accuracy of the active site, the reference ligands were re-docked into their original protein targets. The redocking revealed that the ligands maintained the same interaction patterns as observed in the crystal structures.[24]

Docking studies with Inh A. InhA plays a major role in the type II fatty acid biosynthesis pathway.[7] Tyr158 is an important amino acid residue because it interacts with long-chain fatty acyl substrates, which are required for mycolic acid synthesis in mycobacterium.[25] The majority of the active compounds displayed pi–pi stacking interactions with the Tyr158 and Phe149 residues, along with significant hydrogen bonding interactions with Ile194 and Tyr158. The binding affinities of the most potent *anti*-TB molecules (**K1**, **K2**, and **K3**) are −9.6, −8.9, and −8.8 kcal mol^{-1} respectively as indicated in Table 6 and the docking orientations of these compounds are shown in Fig. 6. Compound **K1** exhibited the highest docking score of −9.6 kcal mol^{-1} with 1P44, implying hydrogen bond interactions with Tyr158 and Ile194 residues. These interactions are mediated by the ester carbonyl oxygen atom and thiazole ring nitrogen atom. Furthermore, a pi–pi stacking interaction was found between the Tyr158 residue and the methyl-substituted phenyl ring (Fig. 6a). Compound **K2** showed a docking score of −8.9 kcal mol^{-1} resulting in hydrogen bond interactions with Tyr158 and Ile194 residues and a pi–pi stacking interaction with Phe149 residue. The Tyr158 residue interacts with the ester carbonyl oxygen atom, whilst the Ile194 residue interacts with

Table 6 Binding energy and interactions of target molecules (K1, K2, and K3) and Co-crystal ligands with receptor 1P44 and 4KTF

	1P44			4KTF		
Compound code	Docking score (kcal mol^{-1})	H-boding	Pi–Pi stacking	Docking score (kcal mol^{-1})	H-boding	Pi–Pi stacking
K1	−9.6	Tyr158, Ile194	Tyr158	−7.2	Gln385	—
K2	−8.9	Tyr158, Ile194	Phe149	−4.5	Gln385	Trp182
K3	−8.8	Tyr158, Ile194	Phe149	−5.4	—	Trp182
GEQ	−9.7	Tyr158	Tyr158, Phe149			
1 TM				−7.2	Gln385. Ala167	Phe168

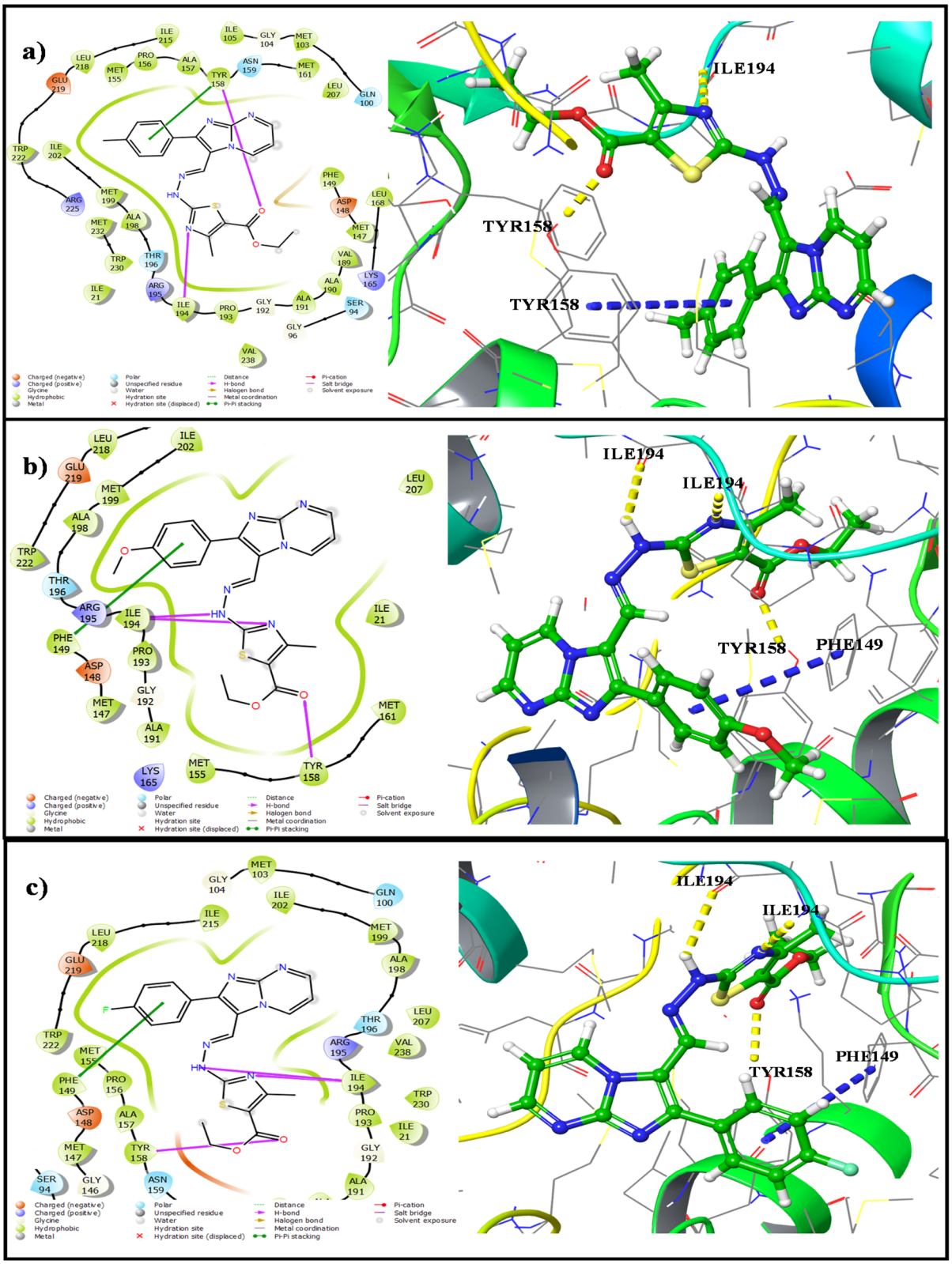

Fig. 6 The 2D (left) and 3D (right) docking poses of compound (a) **K1**, (b) **K2**, and (c) **K3** with receptor 1P44.

one of the NH groups and the thiazole ring's nitrogen atom. A pi–pi stacking linking happens between the methoxy-substituted phenyl ring and the Phe149 residue (Fig. 6b). Compound **K3** has a docking score of −8.8 kcal mol^{-1} because of its hydrogen bond interactions with Tyr158 and Ile194 residues, as well as a pi–pi stacking interaction with Phe149

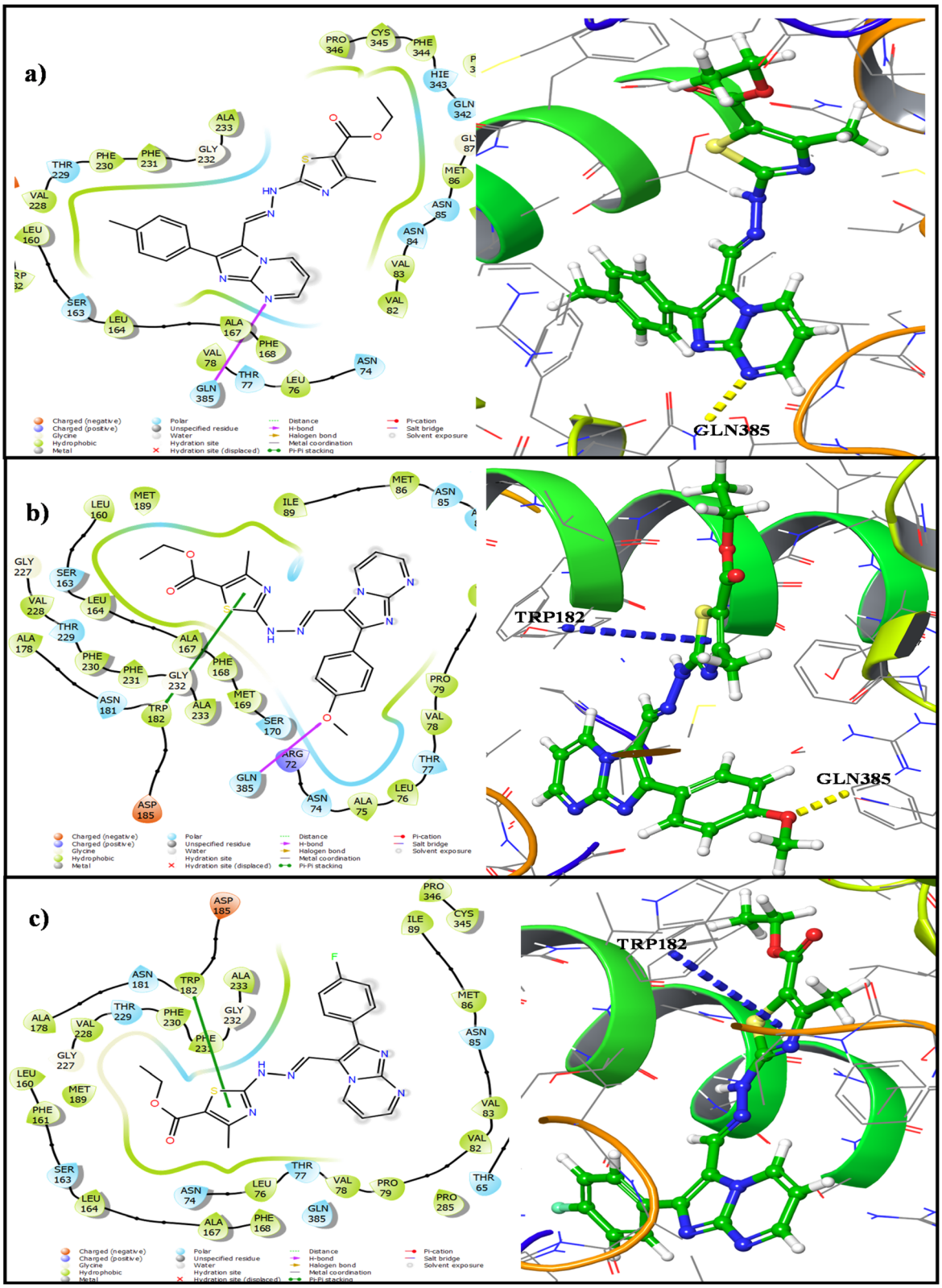

Fig. 7 The 2D (left) and 3D (right) docking poses of compound (a) **K1**, (b) **K2**, and (c) **K3** with receptor 4KTF.

residue. The Tyr 158 residue interacts with the oxygen atom of the ester carbonyl group, whereas the Ile194 residue forms an interaction with the NH group and the nitrogen atom of the thiazole ring. It also forms pi–pi stacking interactions with the Phe149 residue *via* the fluorine-substituted phenyl ring (Fig. 6c).

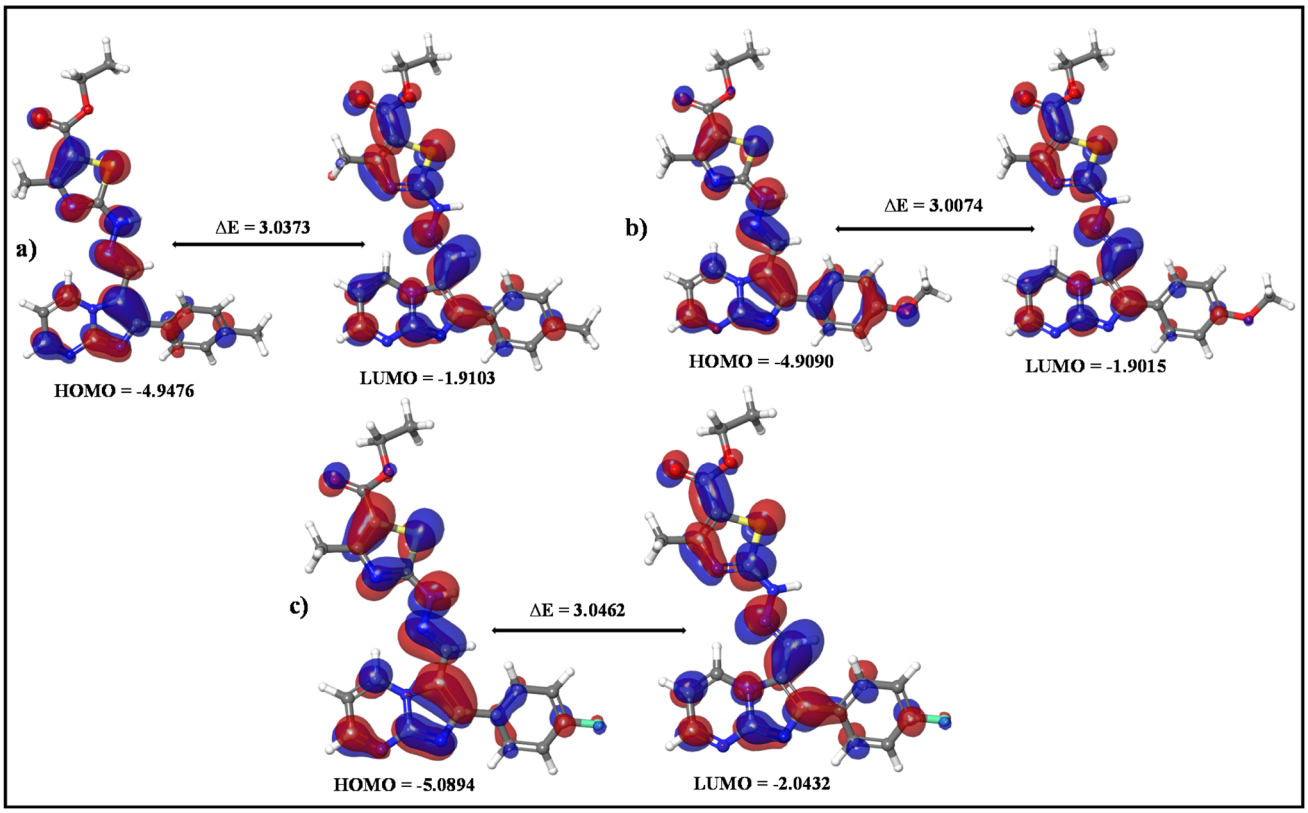

Fig. 8 Frontier molecular orbitals of the compounds (a) K1, (b) K2, and (c) K3.

Docking studies with CYP121. The target compounds formed pi–pi stacking interactions and hydrogen bonding with CYP121 active site amino acid residues. The majority of these compounds interacted with the Trp182 residue through π–π stacking and established hydrogen bonds with the Gln385 residue. The most potent *anti*-TB compounds, **K1**, **K2**, and **K3**, have binding affinities of −7.2, −4.5, and −5.4 kcal mol^{-1}, respectively, as shown in Table 6. Compound **K1** showed the highest docking score (−7.2 kcal mol^{-1}) with 4KTF, indicating hydrogen bond interactions with the Gln385 residue. These interactions are facilitated by one of the nitrogen atoms in the pyrimidine ring (Fig. 7a). Compound **K2** exhibits a docking score of −4.5 kcal mol^{-1}, which is attributable to a hydrogen bond interaction between the Gln385 residue and the oxygen atom of the methoxy group. Furthermore, it produces pi–pi stacking interactions between the Trp182 residue and the thiazole ring (Fig. 7b). Compound **K3** demonstrates a docking score of −5.4 kcal mol^{-1}, reflecting pi–pi stacking interactions between the Trp 182 residue and the thiazole ring (Fig. 7c). Overall, connecting a thiazole ring to the imidazo[1,2-*a*]pyrimidine scaffold increased the possibility of hydrogen bonding and pi–pi stacking interactions with Tyr158, Phe148, Ile194, and Gln385 residues, which are important active sites of the InhA protein. Similar interactions were observed with the CY121 protein's Trp182, and Gln385 residues, which are probably responsible for the hybrid compounds' increased inhibitory effectiveness against the *M. tuberculosis* H37Rv strain.

DFT studies

Drug design requires an understanding of drug-target interactions. Covalent bonds, ionic forces, hydrogen bonds, charge transfer, dipole interactions, and hydrophobic effects are some examples of these interactions. Hydrogen bonds, formed through charge transfer between electron-rich donors and electron-deficient acceptors, as well as hydrophobic

Table 7 The global reactivity parameters of K1–K3 using DFT studies[a]

Comp	HOMO (eV)	LUMO (eV)	Δ*E* (eV)	IP (eV)	EA (eV)	*η* (eV)	*σ* (eV)	*μ* (eV)	*ω* (eV)	*χ* (eV)
K1	−4.9476	−1.9103	3.0373	4.9476	1.9103	1.5186	0.3292	−1.5186	0.7593	3.4289
K2	−4.9090	−1.9015	3.0074	4.9090	1.9015	1.5037	0.3325	−1.5037	0.7518	3.4052
K3	−5.0894	−2.0432	3.0462	5.0894	2.0432	1.5231	0.3282	−1.5231	0.7615	3.5663

[a] Comp.: compound code, bandgap (ΔE) = $E_{HOMO} - E_{LUMO}$, ionization potential (IP) = $-E_{HOMO}$, electron affinity (EA) = $-E_{LUMO}$, chemical hardness (η) = (IP-EA)/2, chemical softness (σ) = 1/2 η, chemical potential (μ) = $-\eta$, electrophilicity index (ω) = η/2, electronegativity (χ) = (IP + EA)/2.

interactions between nonpolar regions are weak forces that frequently stabilize drug-receptor complexes. DFT's ability to reliably estimate the strength of these interactions is critical in determining its efficacy for computer-aided drug creation. In chemical reactions, molecular orbitals are essential for electron transport. The lowest energy orbital is called the LUMO, while the orbital containing the highest-energy electrons is called the HOMO. The energies of the HOMO and LUMO can be used to calculate a variety of chemical properties. These include electron affinity (EA), ionization potential (IP), chemical potential (μ), electronegativity (χ), electrophilicity index (ω), hardness (η), and chemical softness (s). The molecules with a low ΔE value are categorized as soft because of their lower kinetic stability, easier electronic structure adjustment, and increased reactivity. The molecules with a high ΔE value, are considered hard due to their increased kinetic stability, decreased reactivity, and resistance to changes in their electronic configurations. The target compounds HOMO and LUMO frontier orbitals are distributed consistently throughout the molecule. For the compounds **K1**, **K2**, and **K3** the HOMO electron density is distributed over an imidazo[1,2-*a*]pyrimidine and also partially distributed over the imine bond and the –NH group. The LUMO electron density was distributed around both imidazo[1,2-*a*] pyrimidine and thiazole rings (Fig. 8). Molecules **K1**, **K2**, and **K3** were found to have energy band gap values of 3.0373, 3.0074, and 3.0462 eV, respectively (Table 7). EA demonstrates the ability to take electrons, while IP reflects the ability to donate them. All final compounds are more likely to donate electrons than to take them, as indicated by their larger IP compared to EA. It was further confirmed that all final compounds were electron-donating (nucleophilic) since their electronegativity values were lower than their IP.[26] Also, all designed compounds have an electrophilic index lower than their IP, indicating their propensity to receive electrons. This suggests that the majority of the compounds are nucleophilic. The molecular electrostatic potential (MEP) map shows the distribution of electrostatic potential (EP) among atomic sites, considering the partial charge distribution, electronegativity of significant atoms, and their interactions. Fig. 9 and 10 display the MEP characteristics of compounds **K1**, **K2**, and **K3**. The electrostatic potential values are displayed in different colors: red represents regions with a high negative electrostatic potential, blue represents areas with the highest positive electrostatic potential, and green shows regions with zero potential. These molecules' red regions

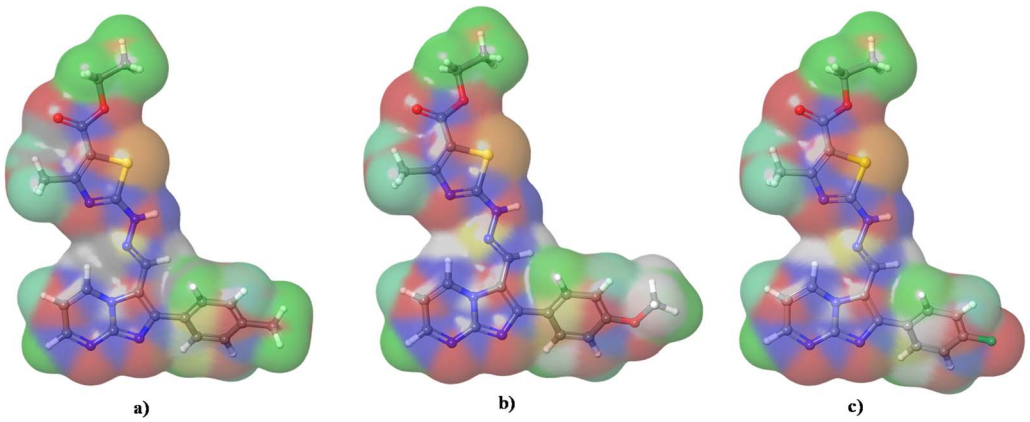

Fig. 9 Electron density surface of the compounds (a) K1 (b) K2 and (c) K3.

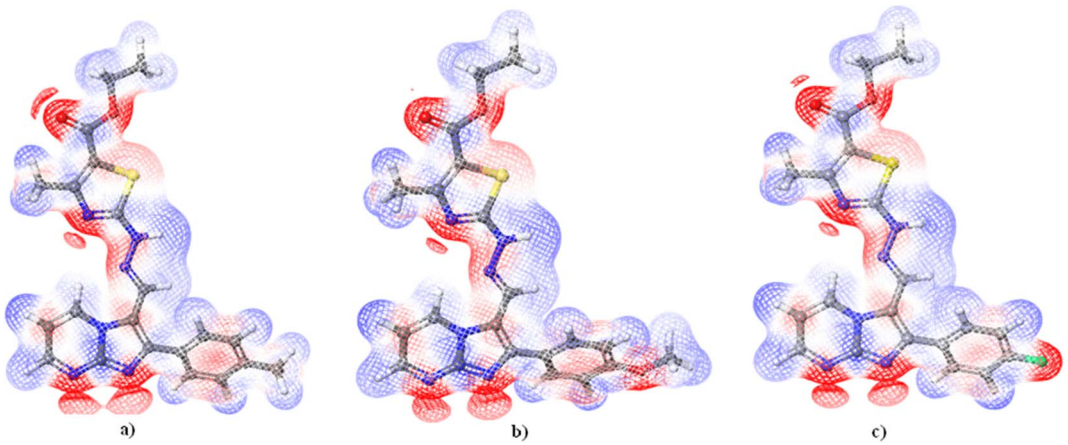

Fig. 10 Electrostatic potential of the compounds (a) K1, (b) K2, and (c) K3.

appear to surround the carbonyl oxygen and nitrogen atoms in the imidazo[1,2-*a*]pyrimidine, thiazole, and hydrazine links, indicating their nucleophilic nature.

Conclusions

Four different series of 26 novel hydrazineyl-linked imidazo [1,2-*a*]pyrimidine-thiazole hybrid compounds (**K1–K26**) were designed using the molecular hybridization technique. The synthesized compounds' structures were confirmed using ^{1}H NMR, ^{13}C NMR, and mass spectrometry investigations. All of the compounds showed encouraging action against the *mycobacterium tuberculosis* H37Rv strain (ATCC 27294) in the anti-tubercular study. Compounds **K1**, **K2**, and **K3** were the most potent, with a MIC of 1.6 μg mL^{-1}. Cytotoxicity investigations found that the *anti*-TB active compounds were non-toxic to normal cell lines (SI > 10), indicating their potential as therapeutic candidates. Furthermore, most of the target compounds demonstrated strong antibacterial activity against all four tested bacterial strains. Additionally, the imidazo[1,2-*a*] pyrimidine-thiazole compounds' significant binding affinity to the target enzymes InhA and CYP121 active sites confirmed their *in vitro* activity profile. According to *in silico* ADME investigations, most of the target compounds have a high oral bioavailability. According to DFT study results, these compounds have electronic characteristics such as a lower electron affinity, a reduced HOMO–LUMO energy gap, high chemical potential, low chemical hardness, and increased chemical softness. These features suggest increased responsiveness and more robust binding interactions with the receptor. Therefore, these imidazo[1,2-*a*]pyrimidine-thiazole derivatives have a lot of potential as lead candidates for the discovery of novel *anti*-TB drugs.

Experimental section

Materials and methods

The chemicals utilized in this investigation were sourced from reliable suppliers such as Sigma Aldrich, TCI, and Alfa Aesar. The reaction process was monitored using thin-layer chromatography (TLC) on alumina plates coated with silica gel (Merck 60 F254) as the stationary phase. The mobile phase was a 1 : 1 combination of ethyl acetate and petroleum ether, and the formed spots were observed using a UV chamber. The melting points of the produced compounds were determined using a digital melting point instrument with no adjustments. Spectroscopic examination was performed using a Bruker FT-NMR spectrometer at 400 MHz for ^{1}H-NMR and 100 MHz for ^{13}C-NMR. Solvents employed included $CDCl_3$ and DMSO-d_6, with tetramethylsilane (TMS) serving as an internal reference. Chemical shifts were recorded in parts per million (δ-scale), while coupling constants were measured in hertz. The ^{1}H-NMR splitting patterns are labeled with conventional abbreviations: "s" (singlet), "d" (doublet), "t" (triplet), "q" (quartet), "m" (multiplet), and "dd" (doublet of doublets). The NMR spectra were examined with Bruker's TopSpin 4.1.4 software. In addition, mass spectra of all intermediate and final compounds were obtained using a Waters Xevo QTOF MS system with electrospray ionization (HR-MS).

Synthesis and characterization

General procedure for the synthesis of 2-aryl imidazo[1,2-*a*] pyrimidines (3a–g). 2-Amino pyrimidine (5 g, 52.60 mmol) and the appropriate substituted phenacyl bromide derivative (2a-2d) (52.60 mmol) were mixed with anhydrous acetone (50 mL) in a clean 250 mL round-bottom flask. The reaction mixture was heated at 70 °C for 12 h. Once the reaction was complete as confirmed by TLC monitoring, the precipitate was filtered, washed with acetone, and dried. Absolute ethanol was used for recrystallization. The isolated product yields ranged between 85–98%.

2-(*p*-tolyl)imidazo[1,2-*a*]pyrimidine (3a). White solid, yield: 9.8 g, 89%; m.p.:294–295 °C; ^{1}H NMR (DMSO-d_6, 400 MHz, δ in ppm) 9.29 (1H, d, J = 6.3 Hz), 8.97 (1H, s), 8.69 (1H, s), 7.91 (2H, d, J = 8.0 Hz), 7.61 (1H, d, J = 4.3 Hz), 7.42 (2H, d, J = 8.0 Hz), 2.39 (3H, s). ^{13}C NMR (DMSO-d_6, 100 MHz, δ in ppm) 157.09, 144.82, 141.03, 138.10, 136.75, 130.49, 126.63, 124.20, 114.26, 109.52, 21.46. HR-MS: m/z calculated for $C_{13}H_{11}N_3$: 209.0953; found: 210.0958 $[M + H]^+$.

2-(4-methoxyphenyl)imidazo[1,2-*a*]pyrimidine (3b). White solid, yield: 11.2 g, 95%; m.p.:187–189 °C; ^{1}H NMR (DMSO-d_6, 400 MHz, δ in ppm) 9.29 (1H, d, J = 6.7 Hz), 8.97 (1H, d, J = 4.4 Hz), 8.65 (1H, s), 7.97 (2H, d, J = 8.6 Hz), 7.62 (1H, q, J = 3.7 Hz), 7.18 (2H, d, J = 8.6 Hz), 3.85 (3H, s). ^{13}C NMR (DMSO-d_6, 100 MHz, δ in ppm) 161.48, 156.84, 144.65, 137.99, 136.59, 128.39, 119.10, 115.41, 114.29, 108.79, 56.00. HR-MS: m/z calculated for $C_{13}H_{11}N_3O$: 225.0902; found: 226.0912 $[M + H]^+$.

2-(4-fluorophenyl)imidazo[1,2-*a*]pyrimidine (3c). White solid, yield: 9.8 g, 87%; m.p.: 226–228 °C; ^{1}H NMR (DMSO-d_6, 400 MHz, δ in ppm) 9.31 (1H, q, J = 2.8 Hz), 8.98 (1H, q, J = 2.0 Hz), 8.73 (1H, s), 8.08 (2H, q, J = 4.7 Hz), 7.60 (1H, q, J = 3.7 Hz), 7.49 (2H, t, J = 8.8 Hz). ^{13}C NMR (DMSO-d_6, 100 MHz, δ in ppm) 164.87, 162.40, 157.05, 145.08, 138.12, 136.24, 129.26, 129.18, 124.05,117.19, 116.97, 114.09, 109.88. HR-MS: m/z calculated for $C_{12}H_8FN_3$; 213.0702; found: 214.0708 $[M + H]^+$.

2-(4-chlorophenyl)imidazo[1,2-*a*]pyrimidine (3d). White solid, yield: 11.6 g, 96%; m.p.: 267–268 °C; ^{1}H NMR (DMSO-d_6, 400 MHz, δ in ppm) 9.28 (1H, d, J = 6.7 Hz), 8.94 (1H, d, J = 4.12 Hz), 8.75 (1H, s), 8.04 (2H, d, J = 8.16 Hz), 7.67 (2H, d, J = 8.12 Hz), 7.55 (1H, q, 4.6 Hz). ^{13}C NMR (DMSO-d_6, 100 MHz, δ in ppm) 156.99, 145.31, 138.08, 136.39, 135.46, 130.00, 128.46, 126.66, 113.93, 110.30. HR-MS: m/z calculated for $C_{12}H_8ClN_3$; found: 229.0407; found: 230.0415 $[M + H]^+$.

2-(4-bromophenyl)imidazo[1,2-*a*]pyrimidine (3e). White solid, yield: 14 g, 97%; m.p.: 287–289 °C; ^{1}H NMR (DMSO-d_6, 400 MHz, δ in ppm) 9.27 (1H, dd, J = 1.4, 6.7 Hz), 8.92 (1H, d, J = 2.9 Hz), 8.74 (1H, s), 7.97 (2H, d, J = 8.5 Hz), 7.81 (2H, d, J = 8.5 Hz), 7.54 (1H, q, J = 3.7 Hz).^{13}C NMR (DMSO-d_6, 100 MHz, δ in ppm) 156.44, 145.60, 137.83, 137.24, 132.82, 128.58, 127.57, 123.98, 113.50, 110.12. HR-MS: m/z calculated for $C_{12}H_8BrN_3$; found: 272.9902; found: 273.9910 $[M + H]^+$.

4-(imidazo[1,2-*a*]pyrimidin-2-yl)benzonitrile (3f). White solid, yield: 9.3 g, 80%; m.p.: 222–223 °C; ^{1}H NMR (DMSO-d_6,

400 MHz, δ in ppm) δ_H 9.23 (1H, dd, J = 1.7, 6.7 Hz), 8.88 (1H, dd, J = 1.6, 4.2 Hz), 8.79 (1H, s), 8.21 (2H, d, J = 8.4 Hz), 8.04 (2H, d, J = 8.4 Hz), 7.46–7.43 (1H, m). ^{13}C NMR (DMSO-d_6, 100 MHz, δ in ppm) 157.20, 145.03, 138.18, 136.83, 131.00, 129.96, 127.22, 126.73, 114.20, 110.01. HR-MS: m/z calculated for $C_{13}H_8N_4$; found: 220.0749; found: 221.0761 $[M + H]^+$.

2-phenylimidazo[1,2-*a*]pyrimidine (3g). White solid, yield: 8.4 g, 82%; m.p.: 272–273 °C; ^{1}H NMR (DMSO-d_6, 400 MHz, δ in ppm) δ_H 9.29 (1H, d, J = 6.1 Hz), 8.97 (1H, d, J = 3.4 Hz), 8.73 (1H, s), 8.02 (2H, d, J = 7.6 Hz), 7.62–7.58 (3H, m), 7.55 (1H, d, J = 7.1 Hz). ^{13}C NMR (DMSO-d_6, 100 MHz, δ in ppm)156.17, 146.32, 137.74, 133.70,127.17, 118.96, 113.01, 112.34, 111.39. HR-MS: m/z calculated for $C_{12}H_9N_3$; found: 195.0796; found: 196.0814 $[M + H]^+$.

General procedure for the synthesis of 2-aryl imidazo[1,2-*a*] pyrimidine-3-carbaldehyde (4a–g). In a clean 100 mL two-neck round-bottom flask, dimethyl formamide (DMF) (6 mL) was added first, followed by phosphorus oxychloride ($POCl_3$) (10 mL) was gradually added while the temperature remained below 10 °C. After 10 min of stirring, compound (**3a–g**) (**6g**) dissolved in DMF (25 mL) was added to the mixture. For 2 h, the reaction mixture was heated at 100 °C. After cooling, it was poured over crushed ice water. A 10% sodium hydroxide (NaOH) solution was added to the reaction mixture to neutralize it. After the solid was separated and filtered, it was thoroughly cleaned with ice-cold water. Compounds (**4a–d**) were obtained by purifying the product by column chromatography using a petroleum ether/ethyl acetate (7 : 3) solvent system.

2-(*p*-tolyl)imidazo[1,2-*a*]pyrimidine-3-carbaldehyde (4a). Off white solid, yield: 5.5 g, 80%; m.p.: 220–221 °C; ^{1}H NMR ($CDCl_3$,400 MHz, δ in ppm) 10.13 (1H, s), 9.90 (1H, dd, J = 2.1, 6.8 Hz), 8.83 (1H, dd, J = 2.1, 4.3 Hz), 7.83 (2H, d, J = 8.1 Hz), 7.37 (2H, d, J = 8.0 Hz), 7.19 (1H, q, J = 3.7 Hz), 2.46 (3H, s). ^{13}C NMR (DMSO-d_6, 100 MHz, δ in ppm)180.29, 159.38, 154.44, 150.38, 140.83, 136.36, 129.91, 129.77, 128.86, 118.84, 111.27, 21.46. HR-MS: m/z calculated for $C_{14}H_{11}N_3O$: 237.0902; found: 238.0918 $[M + H]^+$.

2-(4-methoxyphenyl)imidazo[1,2-*a*]pyrimidine-3-carbaldehyde (4b). White solid, yield: 5.9 g, 88%; m.p.: 188–189 °C; ^{1}H NMR ($CDCl_3$,400 MHz, δ in ppm) 10.12 (1H, s), 9.89 (1H, dd, J = 2.04, 6.8 Hz), 8.82 (1H, dd, J = 2.04, 4.3 Hz), 7.89 (2H, d, J = 8.76 Hz),7.16 (1H, q, J = 4.32 Hz), 7.08 (2H, d, J = 8.76 Hz), 3.90 (3H, s). ^{13}C NMR (DMSO-d_6, 100 MHz, δ in ppm) 180.13, 161.61, 159.08, 154.41, 150.40, 136.34, 131.44, 124.17, 118.61, 114.53, 111.16, 55.47. HR-MS: m/z calculated for $C_{14}H_{11}N_3O_2$: 253.0851; found: 254.0862 $[M + H]^+$.

2-(4-fluorophenyl)imidazo[1,2-*a*]pyrimidine-3-carbaldehyde (4c). Off white solid, yield: 5.3 g, 78%; m.p.: 204–205 °C; ^{1}H NMR ($CDCl_3$,400 MHz, δ in ppm) 10.09 (1H, s), 9.88 (1H, dd, J = 2.04, 6.7 Hz), 8.83 (1H, dd, J = 2,08, 4.3 Hz), 7.91 (2H, d, 3.08 Hz), 7.18 (1H, m). ^{13}C NMR (DMSO-d_6, 100 MHz, δ in ppm) 179.85, 165.51, 163.01, 158.06, 154.67, 150.28, 136.39, 131.93, 131.84, 127.93,127.90, 118.87, 116.35, 116.13, 111.49. HR-MS: m/z calculated for $C_{13}H_8FN_3O$: 241.0651; found: 242.0657 $[M + H]^+$.

2-(4-chlorophenyl)imidazo[1,2-*a*]pyrimidine-3-carbaldehyde (4d). Off white solid, yield: 5.7 g, 85%; m.p.: 214–215 °C; ^{1}H NMR ($CDCl_3$,400 MHz, δ in ppm) 10.05 (1H, s), 9.83 (1H, dd, J = 1.7, 6.7 Hz), 8.79 (1H, dd, J = 1.9, 4.1 Hz), 7.81 (2H, d, J = 8.4 Hz), 7.48 (2H, d, J = 8.4 Hz), 7.15 (1H, q, J = 3.7 Hz). ^{13}C NMR (DMSO-d_6, 100 MHz, δ in ppm)179.75, 157.76, 154.74, 150.28, 136.88, 136.41, 131.15, 130.17, 129.34, 118.97, 111.57. HR-MS: m/z calculated for $C_{13}H_8ClN_3O$: 257.0356; found: 258.0358 $[M + H]^+$.

2-(4-bromophenyl)imidazo[1,2-*a*]pyrimidine-3-carbaldehyde (4e). Off white solid, yield: 5.6 g, 85%; m.p.: 214–215 °C; ^{1}H NMR ($CDCl_3$,400 MHz, δ in ppm) 9.95 (1H, s), 9.73 (1H, dd, J = 2.1, 6.8 Hz), 8.69 (1H, q, J = 2.1 Hz), 7.64 (2H, d, J = 8.4 Hz), 7.54 (2H, t, J = 4.2 Hz), 7.06 (1H, q, J = 3.7 Hz). ^{13}C NMR (DMSO-d_6, 100 MHz, δ in ppm)175.99, 153.09, 149.99, 145.56, 131.66, 127.55, 126.61, 125.90, 120.50, 114.21, 106.81. HR-MS: m/z calculated for $C_{13}H_8BrN_3O$: 300.9851; found: 301.9863 $[M + H]^+$.

4-(3-formylimidazo[1,2-*a*]pyrimidin-2-yl)benzonitrile (4f). Off white solid, yield: 5.3 g, 78%; m.p.: 234–235 °C; ^{1}H NMR ($CDCl_3$,400 MHz, δ in ppm) 10.17 (1H, s), 9.94 (1H, dd, J = 2.1, 6.8 Hz), 8.92 (1H, dd, J = 2.1, 4.2 Hz), 8.08 (2H, d, J = 8.4 Hz), 7.89 (2H, d, J = 8.4 Hz), 7.29 (1H, t, J = 3.4 Hz). ^{13}C NMR (DMSO-d_6, 100 MHz, δ in ppm)179.34, 156.45, 155.12, 150.30, 136.53, 136.11, 132.73, 130.49, 119.39, 118.21, 111.97. HR-MS: m/z calculated for $C_{14}H_8N_4O$: 248.0698; found: 249.0710 $[M + H]^+$.

2-phenylimidazo[1,2-*a*]pyrimidine-3-carbaldehyde (4g). Off white solid, yield: 5.4 g, 80%; m.p.: 176–177 °C; ^{1}H NMR ($CDCl_3$,400 MHz, δ in ppm) 10.15 (1H, s), 9.92 (1H, dd, J = 2.1, 6.8 Hz), 8.86 (1H, dd, J = 2.1, 4.3 Hz), 7.94–7.92 (2H, m), 7.58–7.56 (3H, m), 7.22 (1H, q, J = 3.7 Hz). ^{13}C NMR ($CDCl_3$,100 MHz, δ in ppm) 175.47, 154.40, 149.78, 145.56, 131.62, 126.96, 125.65, 125.25, 124.25, 114.22, 106.65. HR-MS: m/z calculated for $C_{13}H_9N_3O$: 223.0746; found: 224.0758 $[M + H]^+$.

General procedure for the synthesis of (*E*)-2-aryl-imidazo[1,2-*a*]pyrimidin-3-yl)methylene)hydrazinecarbothioamide: (5a–g). In a clean 100 mL round-bottom flask, a solution of 2-aryl-imidazo[1,2-*a*]pyrimidine carbaldehyde (**6g**) in ethanol (40 mL) was taken and thiosemicarbazide (1.0 equivalent) was added along with catalytic quantity of conc HCl (0.5 mL). The reaction mixture was heated to 80 °C for 6–8 h. The resultant suspension was filtered to produce a crude solid, which was then refined by recrystallization from ethanol to yield intermediate (**5a–g**).

(*E*)-2-((2-(*p*-tolyl)imidazo[1,2-*a*]pyrimidin-3-yl)methylene) hydrazinecarbothioamide (5a). Yellow solid, yield: 6.3 g, 80%; m.p.: 220–221 °C; ^{1}H NMR (DMSO-d_6, 400 MHz, δ in ppm) 11.40 (1H, s), 9.92 (1H, d, J = 6.5 Hz), 8.77 (1H, d, J = 1.9 Hz), 8.70 (1H, s), 8.33 (1H, s), 7.94 (1H, s), 7.71 (2H, d, J = 7.5 Hz), 7.39 (2H, d, J = 7.6 Hz), 7.29 (1H, t, J = 5.4 Hz), 2.41 (3H, s). ^{13}C NMR (DMSO-d_6, 100 MHz, δ in ppm) 177.57, 153.42, 149.44, 148.46, 139.60, 138.57, 135.30, 129.92, 129.73, 129.10, 114.02, 111.64, 21.40. HR-MS: m/z calculated for $C_{15}H_{14}N_6S$: 310.1001; found: 311.1018 $[M + H]^+$.

(*E*)-2-((2-(4-methoxyphenyl)imidazo[1,2-*a*]pyrimidin-3-yl) methylene)hydrazine carbothioamide (5b). Yellow solid, yield: 6.6 g, 85%; m.p.: 218–219 °C; ^{1}H NMR (DMSO-d_6, 400 MHz, δ in ppm) 11.38 (1H, s), 9.88 (1H, dd, J = 3.4, 3.4 Hz), 8.70 (2H, m), 8.30 (1H, s), 7.92 (1H, s), 7.76 (2H, d, J = 8.7 Hz), 7.22 (1H, dd, J = 4.3, 6.8 Hz), 7.12 (2H, d, J = 8.7 Hz), 3.85 (3H, s). ^{13}C NMR (DMSO-d_6, 100 MHz, δ in ppm) 177.40, 160.52, 152.39, 151.27, 149.27, 138.18, 135.82, 131.14, 125.48, 114.73, 113.42, 110.83,

55.80. HR-MS: *m*/*z* calculated for $C_{15}H_{14}N_6OS$: 326.0950; found: 327.0962 $[M + H]^+$.

(*E*)-2-((2-(4-fluorophenyl)imidazo[1,2-*a*]pyrimidin-3-yl) methylene)hydrazine carbothioamide (5c). Yellow solid, yield: 6.1 g, 78%; m.p.: 260–261 °C; ^{1}H NMR (DMSO-d_6, 400 MHz, δ in ppm) 11.36 (1H, s), 9.90 (1H, dd, J = 1.7, 6.8 Hz), 8.74 (1H, dd, J = 1.9, 4.2 Hz), 8.68 (1H, s), 8.32 (1H, s), 7.94 (1H, s), 7.87 (2H, q, J = 4.8 Hz), 7.42–7.37 (2H, m), 7.25–7.22 (1H, m). ^{13}C NMR (DMSO-d_6, 100 MHz, δ in ppm) 177.48, 152.72, 150.20, 149.23, 138.33, 135.46, 131.96, 129.64, 116.33, 116.12, 114.04, 111.06. HR-MS: *m*/*z* calculated for $C_{14}H_{11}FN_6S$: 314.0750; found: 315.0758 $[M + H]^+$.

(*E*)-2-((2-(4-chlorophenyl)imidazo[1,2-*a*]pyrimidin-3-yl) methylene)hydrazine carbothioamide (5d). Yellow solid, yield: 6.2 g, 80%; m.p.: 220–221 °C; ^{1}H NMR (DMSO-d_6, 400 MHz, δ in ppm) 11.37 (1H, s), 9.89 (1H, d, J = 6.8 Hz), 8.74 (1H, dd, J = 1.6, 4.0 Hz), 8.69 (1H, s), 8.34 (1H, s), 7.95 (1H, s), 7.83 (2H, d, J = 8.4 Hz), 7.63 (2H, d, J = 8.4 Hz), 7.25–7.23 (1H, m). ^{13}C NMR (DMSO-d_6, 100 MHz, δ in ppm) 177.49, 152.86, 149.80, 149.26, 138.36, 135.33, 134.39, 132.01, 131.43, 129.28, 114.32, 111.13. HR-MS: *m*/*z* calculated for $C_{14}H_{11}ClN_6S$: 330.0454; found: 331.0462 $[M + H]^+$.

(*E*)-2-((2-(4-bromophenyl)imidazo[1,2-*a*]pyrimidin-3-yl) methylene)hydrazine carbothioamide (5e). Yellow solid, yield: 6.4 g, 86%; m.p.: 201–202 °C; ^{1}H NMR (DMSO-d_6, 400 MHz, δ in ppm)11.36 (1H, s), 9.89 (1H, dd, J = 1.7, 6.8 Hz), 8.74 (1H, dd, J = 1.9, 4.2 Hz), 8.68 (1H, s), 8.33 (1H, s), 7.95 (1H, s), 7.75 (4H, s), 7.25–7.23 (1H, m). ^{13}C NMR (DMSO-d_6, 100 MHz, δ in ppm) 177.51, 152.88, 149.86, 149.28, 138.36, 135.32, 132.36, 132.20, 131.69, 123.12, 114.32, 111.13. HR-MS: *m*/*z* calculated for $C_{14}H_{11}BrN_6S$: 373.9949; found: 374.9961$[M + H]^+$.

(*E*)-2-((2-(4-cyanophenyl)imidazo[1,2-*a*]pyrimidin-3-yl) methylene)hydrazinecarbo thioamide (5f). Yellow solid, yield: 5.8 g, 74%; m.p.: 250–251 °C; ^{1}H NMR (DMSO-d_6, 400 MHz, δ in ppm) 11.39 (1H, s), 9.91 (1H, dd, J = 1.7, 6.8 Hz), 8.77 (1H, dd, J = 1.9, 4.2 Hz), 8.76 (1H, s), 8.36 (1H, s), 8.01 (4H, d, J = 3.1 Hz), 7.97 (1H, s), 7.28–7.24 (1H, m). ^{13}C NMR (DMSO-d_6, 100 MHz, δ in ppm) 177.20, 152.90, 148.91, 148.32, 137.31, 132.70, 130.01, 118.74, 114.80, 111.41, 110.95. HR-MS: *m*/*z* calculated for $C_{15}H_{11}N_7S$: 321.0797; found: 322.0807 $[M + H]^+$.

(*E*)-2-((2-phenylimidazo[1,2-*a*]pyrimidin-3-yl)methylene) hydrazinecarbothioamide (5g). Yellow solid, yield: 6.2 g, 78%; m.p.: 244–245 °C; ^{1}H NMR (DMSO-d_6, 400 MHz, δ in ppm) 11.40 (1H, s), 9.91 (1H, dd, J = 1.6, 6.8 Hz), 8.74–8.72 (2H, m), 8.32 (1H, s), 7.94 (1H, s), 7.81 (2H, d, J = 6.9 Hz), 7.68–7.50 (3H, m), 7.25–7.22 (1H, m). ^{13}C NMR (DMSO-d_6, 100 MHz, δ in ppm) 177.50, 152.63, 151.24, 149.30, 138.32, 135.62, 133.14, 129.78, 129.51, 129.23, 114.08, 111.01. HR-MS: *m*/*z* calculated for $C_{14}H_{12}N_6S$: 296.0844; found: 297.0858 $[M + H]^+$.

General procedure for synthesis of (*E*)-2-(2-((2-aryl-imidazo [1,2-*a*]pyrimidin-3-yl)methylene)hydrazineyl)thiazole derivatives (K1–K21). In a clean and dry 50 mL round-bottom flask, appropriately substituted imidazo[1,2-*a*]pyrimidin-3-yl) methylene)hydrazinecarbothioamide (0.5 g) (**5a–g**) was taken in absolute ethanol (20 mL). To this solution, added glacial acetic acid (0.5 mL), triethylamine as a base (1.0 equivalent), and ethyl 2-chloro-3-oxobutanoate/ethyl 3-bromo-2-oxopropanoate/3-chloropentane-2,4-dione (1.5 equivalents). The reaction mixture was then refluxed at 80 °C for 6 h. After completion, the reaction mixture was poured into ice-cold water, and a solid was separated. The crude product was further purified by column chromatography with a (1 : 1) combination of petroleum ether and ethyl acetate as the eluent, yielding compounds **K1–K21**.

Ethyl(*E*)-4-methyl-2-(2-((2-(*p*-tolyl)imidazo[1,2-*a*]pyrimidin-3-yl)methylene)hydrazineyl) thiazole-5-carboxylate (K1). White solid, yield: 0.528 g, 78%; m.p.: 278–279 °C; ^{1}H NMR (DMSO-d_6, 400 MHz, δ in ppm) 12.40 (1H, s), 9.56 (1H, d, J = 6.1 Hz), 8.75 (1H, dd, J = 1.9, 4.2 Hz), 8.59 (1H, s), 7.71 (2H, d, J = 8.0 Hz), 7.48–7.46 (1H, m), 7.38 (2H, d, J = 8.0 Hz), 4.25 (2H, q, J = 7.1 Hz), 2.46 (3H, s), 2.41 (3H, s), 1.30 (3H, t, J = 7.1 Hz). ^{13}C NMR (DMSO-d_6, 100 MHz, δ in ppm) 162.25, 152.23, 150.59, 149.18, 139.16, 135.66, 130.39, 129.85, 129.49, 114.11, 111.06, 60.66, 21.36, 14.80. HR-MS: *m*/*z* calculated for $C_{21}H_{20}N_6O_2S$: 420.1368; found: 421.1362 $[M + H]^+$.

Ethyl(*E*)-2-(2-((2-(4-methoxyphenyl)imidazo[1,2-*a*]pyrimidin-3-yl)methylene)hydrazineyl)-4-methylthiazole-5-carboxylate (K2). White solid, yield: 0.534 g, 80%; m.p.: 252–253 °C; ^{1}H NMR (DMSO-d_6, 400 MHz, δ in ppm) 12.42 (1H, s), 9.54 (1H, d, J = 6.3 Hz), 8.74 (1H, dd, J = 1.9, 4.1 Hz), 8.58 (1H, s), 7.76 (2H, d, J = 8.7 Hz), 7.46 (1H, q, J = 3.7 Hz), 7.13 (2H, d, J = 8.7 Hz), 4.25 (2H, q, J = 7.1 Hz), 3.85 (3H, s), 2.46 (3H, s), 1.30 (3H, t, J = 7.1 Hz). ^{13}C NMR (DMSO-d_6, 100 MHz, δ in ppm) 168.03, 161.39, 160.48, 151.96, 149.87, 148.99, 135.44, 134.18, 130.93, 125.63, 118.90, 114.81, 113.77, 110.83, 60.91, 55.79, 14.64. HR-MS: *m*/*z* calculated for $C_{21}H_{20}N_6O_3S$: 436.1318; found: 437.1311$[M + H]^+$.

Ethyl(*E*)-2-(2-((2-(4-fluorophenyl)imidazo[1,2-*a*]pyrimidin-3-yl)methylene)hydrazineyl)-4-methylthiazole-5-carboxylate (K3). White solid, yield: 0.500 g, 74%; m.p.: 248–249 °C; ^{1}H NMR (DMSO-d_6, 400 MHz, δ in ppm) 12.33 (1H, s), 9.53 (1H, d, J = 6.7 Hz), 8.75 (1H, dd, J = 1.6, 3.8 Hz), 8.55 (1H, s), 7.83 (2H, d, J = 8.4 Hz), 7.63 (2H, t, J = 4.2 Hz), 7.47–7.44 (1H, m), 4.24 (2H, q, J = 7.0 Hz), 2.44 (3H, s), 1.30 (3H, t, J = 7.1 Hz). ^{13}C NMR (DMSO-d_6, 100 MHz, δ in ppm) 162.22, 152.59, 149.12, 148.90, 135.75, 134.41, 132.09, 131.22, 129.31, 114.59, 111.27, 60.69, 14.79. HR-MS: *m*/*z* calculated for $C_{20}H_{17}FN_6O_2S$: 424.1118; found: 425.1110 $[M + H]^+$.

Ethyl(*E*)-2-(2-((2-(4-chlorophenyl)imidazo[1,2-*a*]pyrimidin-3-yl)methylene)hydrazineyl)-4-methylthiazole-5-carboxylate (K4). Yellow solid, yield: 0.500 g, 75%; m.p.: 262–263 °C; ^{1}H NMR (DMSO-d_6, 400 MHz, δ in ppm) 12.37 (1H, s), 9.52 (1H, d, J = 6.1 Hz), 8.75 (1H, dd, J = 1.9, 4.1 Hz), 8.54 (1H, s), 7.75 (4H, s), 7.47 (1H, q, J = 3.7 Hz), 4.24 (3H, q, J = 7.1 Hz), 2.44 (3H, s), 1.30 (3H, t, J = 7.1 Hz). ^{13}C NMR (DMSO-d_6, 100 MHz, δ in ppm) 162.20, 152.56, 149.10, 148.86, 135.73, 134.39, 132.08, 131.21, 129.30, 114.56, 111.26, 60.68, 14.79. HR-MS: *m*/*z* calculated for $C_{20}H_{17}ClN_6O_2S$: 440.0822; found: 441.0832 $[M + H]^+$.

Ethyl(*E*)-2-(2-((2-(4-bromophenyl)imidazo[1,2-*a*]pyrimidin-3-yl)methylene)hydrazineyl)-4-methylthiazole-5-carboxylate (K5). Yellow solid, yield: 0.582 g, 90%; m.p.: 285–286 °C; ^{1}H NMR (DMSO-d_6, 400 MHz, δ in ppm) 12.34 (1H, s), 9.51 (1H, d, J = 5.9 Hz), 8.73 (1H, s), 8.53 (1H, s), 7.85 (2H, m), 7.44–7.37 (3H, m), 4.23 (2H, d, J = 6.9 Hz), 2.43 (3H, s), 1.28 (3H, t, J = 6.8 Hz). ^{13}C NMR (DMSO-d_6, 100 MHz, δ in ppm) 162.24, 161.90, 152.47,

149.36, 149.11, 135.73, 131.77, 131.69, 129.75, 116.39, 116.17, 114.33, 111.24, 60.68, 14.79. HR-MS: *m*/*z* calculated for $C_{20}H_{17}BrN_6O_2S$: 484.0317; found: 485.0325 $[M + H]^+$.

Ethyl(*E*)-2-(2-((2-(4-cyanophenyl)imidazo[1,2-*a*]pyrimidin-3-yl)methylene)hydrazineyl)-4-methylthiazole-5-carboxylate (K6). Yellow solid, yield: 0.498 g, 74%; m.p.: 183–184 °C; ^{1}H NMR (DMSO-d_6, 400 MHz, δ in ppm) 12.41 (1H, s), 9.55 (1H, d, $J = 6.6$ Hz), 8.78 (1H, d, $J = 2.0$ Hz), 8.58 (1H, s), 8.01 (4H, s), 7.50 (1H, q, $J = 3.6$ Hz), 4.25 (2H, q, $J = 7.0$ Hz), 2.45 (3H, s), 1.30 (3H, t, $J = 7.0$ Hz). ^{13}C NMR (DMSO-d_6, 100 MHz, δ in ppm) 162.22, 153.10, 149.19, 147.82, 137.79, 135.96, 133.16, 130.22, 119.11, 115.47, 111.84, 60.74, 14.80. HR-MS: *m*/*z* calculated for $C_{21}H_{17}N_7O_2S$: 431.1164; found: 432.1172 $[M + H]^+$.

Ethyl(*E*)-4-methyl-2-(2-((2-phenylimidazo[1,2-*a*]pyrimidin-3-yl)methylene)hydrazineyl) thiazole-5-carboxylate (K7). Yellow solid, yield: 0.494 g, 72%; m.p.: 212–213 °C; ^{1}H NMR (DMSO-d_6, 400 MHz, δ in ppm) 12.41 (1H, s), 9.55 (1H, d, $J = 6.36$ Hz), 8.75 (1H, t, 1.24 Hz), 8.59 (1H, s), 7.80 (2H, d, $J = 7.72$ Hz), 7.59–7.51 (3H, m), 7.46 (1H, q, $J = 4.6$ Hz), 4.22 (2H, q, $J = 7.0$ Hz), 2.44 (3H, s), 1.28 (3H, t, $J = 7.08$ Hz). ^{13}C NMR (DMSO-d_6, 100 MHz, δ in ppm) 162.24, 152.36, 150.45, 149.18, 135.73, 133.23, 129.63, 129.50, 129.26, 114.387, 111.15, 60.66, 14.79. HR-MS: *m*/*z* calculated for $C_{20}H_{18}N_6O_2S$: 406.1212; found: 407.1216 $[M + H]^+$.

Ethyl(*E*)-2-(2-((2-(*p*-tolyl)imidazo[1,2-*a*]pyrimidin-3-yl) methylene)hydrazineyl)thiazole-5-carboxylate (K8). Yellow solid, yield: 0.582 g, 89%; m.p.: 200–201 °C; ^{1}H NMR (DMSO-d_6, 400 MHz, δ in ppm) 12.37 (1H, s), 9.53 (1H, s), 8.76 (1H, s), 8.56 (1H, s), 7.83 (2H, d, $J = 5.9$ Hz), 7.63 (2H, d, $J = 6.1$ Hz), 7.47 (1H, s), 4.23 (2H, d, $J = 5.2$ Hz), 2.45 (3H, s), 1.29 (3H, s). ^{13}C NMR (DMSO-d_6, 100 MHz, δ in ppm) 168.02, 161.39, 152.33, 148.87, 139.25, 135.62, 134.03, 130.243, 129.95, 129.49, 118.99, 114.21, 111.10, 60.92, 21.37, 14.65. HR-MS: *m*/*z* calculated for $C_{20}H_{18}N_6O_2S$: 406.1212; found: 407.1218 $[M + H]^+$.

Ethyl(*E*)-2-(2-((2-(4-methoxyphenyl)imidazo[1,2-*a*]pyrimidin-3-yl)methylene)hydrazineyl) thiazole-5-carboxylate (K9). Yellow solid, yield: 0.530 g, 82%; m.p.: 260–261 °C; ^{1}H NMR (DMSO-d_6, 400 MHz, δ in ppm) 12.25 (1H, s), 9.58 (1H, d, $J = 5.1$ Hz), 8.73 (1H, d, $J = 2.2$ Hz), 8.52 (1H, s),7.82 (1H, s), 7.77 (2H, d, $J = 8.5$ Hz), 7.41 (1H, q, $J = 3.6$ Hz), 7.14 (2H, d, $J = 8.5$ Hz), 4.28 (2H, q, $J = 7.0$ Hz), 3.85 (3H, s), 1.31 (3H, t, $J = 7.0$ Hz). ^{13}C NMR (DMSO-d_6, 100 MHz, δ in ppm) 168.03, 161.39, 160.48, 151.96, 149.87, 148.99, 135.44, 134.18, 130.93, 125.63, 118.90, 114.81, 113.77, 110.83, 60.91, 55.79, 14.64. HR-MS: *m*/*z* calculated for $C_{20}H_{18}N_6O_3S$: 422.1161; found: 423.1167 $[M + H]^+$.

Ethyl(*E*)-2-(2-((2-(4-fluorophenyl)imidazo[1,2-*a*]pyrimidin-3-yl)methylene)hydrazineyl) thiazole-5-carboxylate (K10). Orange solid, yield: 0.600 g, 92%; m.p.: 174–175 °C; ^{1}H NMR (DMSO-d_6, 400 MHz, δ in ppm) 12.29 (2H, s), 9.56 (1H, d, $J = 6.9$ Hz), 8.76–8.75 (1H, m), 8.49 (1H, s), 7.84–7.81 (3H, m), 7.64 (2H, d, $J = 8.1$ Hz), 7.43–7.40 (1H, m), 4.28 (2H, q, $J = 6.8$ Hz), 1.31 (3H, t, $J = 6.9$ Hz). ^{13}C NMR (DMSO-d_6, 100 MHz, δ in ppm) 167.97, 164.32, 161.87, 161.36, 152.32, 148.93, 148.68, 135.58, 133.77, 131.65, 129.83, 129.80, 118.98, 116.44, 116.22, 114.36, 111.06, 60.92, 14.64. HR-MS: *m*/*z* calculated for $C_{19}H_{15}FN_6O_2S$: 410.0961; found: 411.0968 $[M + H]^+$.

Ethyl(*E*)-2-(2-((2-(4-chlorophenyl)imidazo[1,2-*a*]pyrimidin-3-yl)methylene)hydrazineyl) thiazole-5-carboxylate (K11). Orange solid, yield: 0.672 g, 96%; m.p.: 240–241 °C; ^{1}H NMR (DMSO-d_6, 400 MHz, δ in ppm) 12.26 (1H, s), 9.56 (1H, dd, $J = 3.4$, 3.4 Hz), 8.75 (1H, d, $J = 2.0$ Hz), 8.48 (1H, s), 7.87 (2H, q, $J = 4.7$ Hz), 7.80 (1H, s), 7.44–7.39 (3H, m), 4.28 (2H, q, $J = 7.1$ Hz), 1.31 (3H, t, $J = 7.1$ Hz). ^{13}C NMR (DMSO-d_6, 100 MHz, δ in ppm) 167.97, 152.51, 148.99, 148.29, 135.67, 134.39, 133.69,131.22, 129.39, 119.06, 114.67, 111.16, 60.93, 14.65. HR-MS: *m*/*z* calculated for $C_{19}H_{15}ClN_6O_2S$: 426.0666; found: 427.0671 $[M + H]^+$.

Ethyl(*E*)-2-(2-((2-(4-bromophenyl)imidazo[1,2-*a*]pyrimidin-3-yl)methylene)hydrazine) thiazole-5-carboxylate (K12). Orange solid, yield: 0.596 g, 95%; m.p.: 254–255 °C; ^{1}H NMR (DMSO-d_6, 400 MHz, δ in ppm) 12.28 (1H, s), 9.55 (1H, dd, $J = 1.64$, 5.2 Hz), 8.75 (1H, dd, $J = 1.76$ Hz), 8.48 (1H, s), 7.81 (1H, s), 7.76 (4H, s), 7.42 (1H, q, $J = 4.2$ Hz) 4.28 (2H, q, $J = 7.04$ Hz), 1.30 (3H, t, $J = 7.12$ Hz). ^{13}C NMR (DMSO-d_6, 100 MHz, δ in ppm) 167.95, 161.36, 152.51, 148.99, 148.31, 135.66, 133.63, 132.54, 132.31, 131.47, 123.10, 119.06, 114.64, 111.15, 60.93, 14.65. HR-MS: *m*/*z* calculated for $C_{19}H_{15}BrN_6O_2S$: 470.0161; found: 471.0154 $[M + H]^+$.

Ethyl(*E*)-2-(2-((2-(4-cyanophenyl)imidazo[1,2-*a*]pyrimidin-3-yl)methylene)hydrazineyl) thiazole-5-carboxylate (K13). Yellow solid, yield: 0.560 g, 86%; m.p.: 168–169 °C; ^{1}H NMR (DMSO-d_6, 400 MHz, δ in ppm) 12.34 (1H, s), 9.58 (1H, dd, $J = 1.9$, 6.9 Hz), 8.79 (1H, dd, $J = 1.9$, 4.1 Hz), 8.51 (1H, s), 8.06 (4H, q, $J = 7.4$ Hz), 7.83 (1H, s), 7.46 (1H, q, $J = 3.7$ Hz), 4.28 (2H, q, $J = 7.1$ Hz), 1.31 (3H, t, $J = 7.1$ Hz). ^{13}C NMR (DMSO-d_6, 100 MHz, δ in ppm) 162.24, 152.37, 150.45, 149.18, 135.74, 133.23, 129.63, 129.51, 129.27, 114.36, 111.17, 60.67, 14.80. HR-MS: *m*/*z* calculated for $C_{20}H_{15}N_7O_2S$: 417.1008; found: 418.1002 $[M + H]^+$.

Ethyl(*E*)-2-(2-((2-phenylimidazo[1,2-*a*]pyrimidin-3-yl) methylene)hydrazineyl)thiazole-5-carboxylate (K14). Yellow solid, yield: 0.530 g, 80%; m.p.: 206–207 °C; ^{1}H NMR (DMSO-d_6, 400 MHz, δ in ppm) 12.27 (1H, s), 9.59 (1H, d, $J = 6.7$ Hz), 8.75 (1H, d, $J = 2.2$ Hz), 8.53 (1H, s), 7.81 (3H, d, $J = 5.7$ Hz), 7.60–7.56 (2H, m), 7.54 (1H, q, $J = 3.6$ Hz), 7.43 (1H, m), 4.28 (2H, q, $J = 7.0$ Hz), 1.31 (4H, t, $J = 7.0$ Hz). ^{13}C NMR (DMSO-d_6, 100 MHz, δ in ppm) 168.01, 161.38, 152.26, 149.77, 149.01, 143.50, 135.62, 133.98, 133.30, 129.60, 129.48, 129.33, 118.97, 114.43, 111.03, 60.91, 14.64. HR-MS: *m*/*z* calculated for $C_{19}H_{16}N_6O_2S$: 392.1055; found: 393.1068 $[M + H]^+$.

(*E*)-1-(4-methyl-2-(2-((2-(*p*-tolyl)imidazo[1,2-*a*]pyrimidin-3-yl) methylene)hydrazineyl) thiazol-5-yl)ethan-1-one (K15). Yellow solid, yield: 0.504 g, 80%; m.p.: 308–309 °C; ^{1}H NMR (DMSO-d_6, 400 MHz, δ in ppm) 12.40 (1H, d, $J = 4.0$ Hz), 9.59 (1H, d, $J = 6.2$ Hz), 8.76 (1H, dd, $J = 1.9$, 4.2 Hz), 8.61 (1H, s), 7.71 (2H, d, $J = 8.0$ Hz), 7.49 (1H, q, $J = 3.7$ Hz), 7.39 (2H, d, $J = 8.0$ Hz), 2.44 (3H, s), 2.41 (3H, s). ^{13}C NMR (DMSO-d_6, 100 MHz, δ in ppm) 189.09, 160.52, 152.29, 152.16, 150.70, 150.65, 149.21, 139.19, 135.77, 135.69, 130.98, 130.38, 129.87, 129.51, 125.55, 114.77, 111.12, 111.02, 29.74, 21.37. HR-MS: *m*/*z* calculated for $C_{20}H_{18}N_6OS$: 390.1263; found: 391.1272 $[M + H]^+$.

(*E*)-1-(2-(2-((2-(4-methoxyphenyl)imidazo[1,2-*a*]pyrimidin-3-yl)methylene)hydrazineyl)-4-methylthiazol-5-yl)ethan-1-one (K16). Yellow solid, yield: 0.480 g, 77%; m.p.: 216–217 °C; ^{1}H NMR (DMSO-d_6, 400 MHz, δ in ppm) 12.40 (1H, s), 9.58 (1H, d, $J = 5.1$ Hz), 8.74 (1H, d, $J = 2.2$ Hz), 8.60 (1H, s), 7.77 (2H, d, $J = 8.5$ Hz), 7.48 (1H, q, $J = 3.6$ Hz), 7.14 (2H, d, $J = 8.5$ Hz), 3.85 (4H,

s), 2.43 (4H, s). ^{13}C NMR (DMSO-d_6, 100 MHz, δ in ppm) 189.20, 160.57, 152.28, 150.74, 149.27, 135.76, 131.01, 125.56, 114.84, 111.12, 55.81, 29.80. HR-MS: m/z calculated for $C_{20}H_{18}N_6O_2S$: 406.1212; found: 407.1220 $[M + H]^+$.

(*E*)-1-(2-(2-((2-(4-fluorophenyl)imidazo[1,2-*a*]pyrimidin-3-yl) methylene)hydrazineyl)-4-methylthiazol-5-yl)ethan-1-one (K17). Yellow solid, yield: 0.440 g, 70%; m.p.: 284–285 °C; ^{1}H NMR (DMSO-d_6, 400 MHz, δ in ppm) 12.48 (1H, s), 12.48 (1H, s), 9.60 (1H, d, $J = 6.0$ Hz), 8.75 (1H, s), 8.65 (1H, s), 7.72 (2H, d, $J = 7.6$ Hz), 7.50–7.47 (1H, m), 7.38 (2H, d, $J = 7.6$ Hz), 2.43 (3H, s), 2.41 (3H, s). ^{13}C NMR (DMSO-d_6, 100 MHz, δ in ppm) 189.13, 164.37, 161.91, 152.53, 149.46, 149.13, 135.84, 131.79, 131.70, 129.74, 116.40, 116.19, 114.37, 29.72. HR-MS: m/z calculated for $C_{19}H_{15}FN_6OS$: 394.1012; found: 395.1017 $[M + H]^+$.

(*E*)-1-(2-(2-((2-(4-chlorophenyl)imidazo[1,2-*a*]pyrimidin-3-yl) methylene)hydrazineyl)-4-methylthiazol-5-yl)ethan-1-one (K18). Yellow solid, yield: 0.498 g, 80%; m.p.: 230–231 °C; ^{1}H NMR (DMSO-d_6, 400 MHz, δ in ppm) 12.45 (1H, s), 9.59 (1H, d, $J = 6.2$ Hz), 8.78 (1H, dd, $J = 2.0$, 4.2 Hz), 8.58 (1H, s), 7.85 (2H, d, $J = 8.5$ Hz), 7.64 (2H, d, $J = 8.5$ Hz), 7.52–7.49 (1H, m), 2.43 (3H, s). ^{13}C NMR (DMSO-d_6, 100 MHz, δ in ppm) 189.17, 152.70, 149.19, 149.08, 135.90, 134.45, 132.11, 131.27, 129.37, 114.68, 111.38, 29.75. HR-MS: m/z calculated for $C_{19}H_{15}ClN_6OS$: 410.0717; found: 411.0724 $[M + H]^+$.

(*E*)-1-(2-(2-((2-(4-bromophenyl)imidazo[1,2-*a*]pyrimidin-3-yl) methylene)hydrazineyl)-4-methylthiazol-5-yl)ethan-1-one (K19). Yellow solid, yield: 0.512 g, 84%; m.p.: 297–298 °C; ^{1}H NMR (DMSO-d_6, 400 MHz, δ in ppm) 12.44 (1H, s), 9.59 (1H, d, $J = 5.84$ Hz), 8.78 (1H, dd, $J = 1.96$ Hz), 8.58 (1H, s), 7.77 (4H, s), 7.52 (1H, q, $J = 4.24$ Hz), 2.43 (3H, s). ^{13}C NMR (DMSO-d_6, 100 MHz, δ in ppm) 189.21, 152.75, 149.22, 149.16, 135.93, 132.47, 132.31, 131.53, 123.19, 114.69, 111.41, 29.78. HR-MS: m/z calculated for $C_{19}H_{15}BrN_6OS$: 454.0211; found: 455.0220 $[M + H]^+$.

(*E*)-4-(3-((2-(5-acetyl-4-methylthiazol-2-yl)hydrazineylidene) methyl)imidazo[1,2-*a*] pyrimidin-2-yl)benzonitrile (K20). Yellow solid, yield: 0.468 g, 75%; m.p.: 270–271 °C; ^{1}H NMR (DMSO-d_6, 400 MHz, δ in ppm) 12.41 (1H, s), 9.89 (1H, s), 9.56 (1H, d, $J = 5.5$ Hz), 8.72 (1H, s), 8.59 (1H, s), 7.65 (2H, d, $J = 8.1$ Hz), 7.46 (1H, t, $J = 5.3$ Hz), 6.95 (2H, d, $J = 8.1$ Hz), 2.50 (3H, s), 2.42 (3H, s). ^{13}C NMR (DMSO-d_6, 100 MHz, δ in ppm) 189.27, 153.19, 148.03, 137.82, 136.10, 133.21, 130.27, 111.88, 111.55 29.47. HR-MS: m/z calculated for $C_{20}H_{15}N_7OS$: 401.1059; found: 402.1068 $[M + H]^+$.

(*E*)-1-(4-methyl-2-(2-((2-phenylimidazo[1,2-*a*]pyrimidin-3-yl) methylene)hydrazineyl) thiazol-5-yl)ethan-1-one (K21). Yellow solid, yield: 0.516 g, 81%; m.p.: 149–150 °C; ^{1}H NMR (DMSO-d_6, 400 MHz, δ in ppm) 12.41 (1H, s), 9.59 (1H, d, $J = 6.3$ Hz), 8.76 (1H, dd, $J = 1.9$, 1.9 Hz), 8.60 (1H, s), 7.82 (2H, d, $J = 7.4$ Hz), 7.59–7.52 (3H, m), 7.49 (1H, q, $J = 3.7$ Hz), 2.48 (3H, s), 2.42 (3H, s). ^{13}C NMR (DMSO-d_6, 100 MHz, δ in ppm) 189.22, 152.52, 150.65, 149.27, 135.90, 133.23, 129.66, 129.58, 129.33, 111.31, 29.79. HR-MS: m/z calculated for $C_{19}H_{16}N_6O_S$: 376.1106; found: 377.1112 $[M + H]^+$.

General procedure for the synthesis of (*E*)-ethyl 2-(4-oxo-2-((*E*)-2-((2-aryl-imidazo[1,2-*a*]pyrimidin-3- yl)methylene)hydrazinyl)thiazol-5(4*H*)-ylidene)acetate (S22–S26). In a clean 50 mL round-bottom flask, the substituted imidazo[1,2-*a*]pyrimidin-3-yl)methylene)hydrazinecarbothioamide (5a-5g) (0.5 g) was dissolved in methanol (20 mL). Diethyl but-2-ynedioate (1.5 equivalent) was then added to the solution, and the reaction was refluxed at 80 °C for 6 h. TLC monitoring confirmed the completion of the reaction, and the reaction mixture was poured into ice-cold water to isolate the required product. The desired product was refined using the recrystallization process with absolute ethanol as a solvent.

Ethyl(*E*)-2-(4-oxo-2-(2-((E)-(2-(*p*-tolyl)imidazo[1,2-*a*] pyrimidin-3-yl)methylene) hydrazineyl)thiazol-5(4*H*)-ylidene) acetate (K22). Orange solid, yield: 0.560 g, 80%; m.p.: 287–289 °C; ^{1}H NMR (DMSO-d_6, 400 MHz, δ in ppm) 12.95 (1H, s), 9.65 (1H, dd, $J = 1.8$, 6.8 Hz), 8.81 (1H, dd, $J = 1.9$, 4.2 Hz), 8.77 (1H, s), 7.75 (2H, d, $J = 8.0$ Hz), 7.51 (1H, dd, $J = 4.3$, 6.8 Hz), 7.40 (2H, d, $J = 7.9$ Hz), 6.68 (1H, s), 4.31 (2H, q, $J = 7.1$ Hz), 2.40 (3H, s), 1.32 (3H, t, $J = 7.1$ Hz). ^{13}C NMR (DMSO-d_6, 100 MHz, δ in ppm) 165.70, 153.26, 149.94, 148.89, 142.75, 139.59, 136.32, 130.06, 129.96, 129.67, 115.21, 114.14, 111.34, 21.42, 14.50. HR-MS: m/z calculated for $C_{21}H_{18}N_6O_3S$: 434.1161; found: 435.1158 $[M + H]^+$.

Ethyl(*E*)-2-(2-(2-((E)-(2-(4-methoxyphenyl)imidazo[1,2-*a*] pyrimidin-3-yl)methylene) hydrazineyl)-4-oxothiazol-5(4*H*)-ylidene)acetate: (K23). Orange solid, yield: 0.540 g, 78%; m.p.: 272–273 °C; ^{1}H NMR (DMSO-d_6, 400 MHz, δ in ppm) 12.87 (1H, s), 9.56 (1H, d, $J = 4.7$ Hz), 8.75 (2H, d, $J = 20.4$ Hz), 7.81 (2H, d, $J = 7.1$ Hz), 7.42 (1H, s), 7.12 (2H, d, $J = 7.0$ Hz), 6.63 (1H, s), 4.26 (2H, d, $J = 6.2$ Hz), 3.85 (3H, s), 1.30 (3H, s). ^{13}C NMR (DMSO-d_6, 100 MHz, δ in ppm) 165.80, 153.08, 149.93, 136.26, 131.18, 125.24, 114.88, 113.89, 111.23, 61.85, 55.78, 14.52. HR-MS: m/z calculated for $C_{21}H_{18}N_6O_4S$: 450.1110; found: 451.1192 $[M + H]^+$.

Ethyl(*E*)-2-(2-(2-((E)-(2-(4-fluorophenyl)imidazo[1,2-*a*] pyrimidin-3-yl)methylene) hydrazineyl)-4-oxothiazol-5(4*H*)-ylidene)acetate (K24). Orange solid, yield: 0.522 g, 75%; m.p.: 270–271 °C; ^{1}H NMR (DMSO-d_6, 400 MHz, δ in ppm) 12.94 (1H, s), 9.63 (1H, d, $J = 6.0$ Hz), 8.81 (1H, s), 8.75 (1H, s), 7.79 (5H, d, $J = 5.8$ Hz), 7.50 (1H, t, $J = 5.3$ Hz), 6.65 (1H, s), 4.28 (3H, d, $J = 6.8$ Hz), 1.32 (4H, t, $J = 6.8$ Hz). ^{13}C NMR (DMSO-d_6, 100 MHz, δ in ppm) 165.78, 153.51, 151.40, 149.83, 136.40, 132.36, 132.14, 131.67, 123.54, 114.96, 114.66, 111.52, 61.87, 14.52. HR-MS: m/z calculated for $C_{20}H_{15}FN_6O_3S$: 438.0910; found: 439.0916 $[M + H]^+$.

Ethyl(*E*)-2-(2-(2-((*E*)-(2-(4-chlorophenyl)imidazo[1,2-*a*] pyrimidin-3-yl)methylene) hydrazineyl)-4-oxothiazol-5(4*H*)-ylidene)acetate (K25). Orange solid, yield: 0.564 g, 82%; m.p.: 282–283 °C; ^{1}H NMR (DMSO-d_6, 400 MHz, δ in ppm) 12.86 (1H, s), 9.59 (1H, d, $J = 4.6$ Hz), 8.79 (1H, s), 8.71 (1H, s), 7.86 (2H, d, $J = 6.9$ Hz), 7.63 (2H, d, $J = 6.9$ Hz), 7.46 (1H, s), 6.63 (1H, s), 4.27 (2H, d, $J = 5.9$ Hz), 1.30 (3H, s). ^{13}C NMR (DMSO-d_6, 100 MHz, δ in ppm) 165.68, 153.43, 151.39, 149.79, 148.24, 142.92.136.32, 134.75, 131.39, 129.39, 115.01, 114.58, 111.46, 61.87, 14.49. HR-MS: m/z calculated for $C_{20}H_{15}ClN_6O_3S$: 454.0615; found: 455.0620 $[M + H]^+$.

Ethyl(*E*)-2-(2-(2-((*E*)-(2-(4-bromophenyl)imidazo[1,2-*a*] pyrimidin-3-yl)methylene) hydrazineyl)-4-oxothiazol-5(4*H*)-ylidene)acetate (K26). Orange solid, yield: 0.572 g, 86%; m.p.: 287–288 °C; ^{1}H NMR (DMSO-d_6, 400 MHz, δ in ppm) 12.85 (1H, s), 9.60 (1H, d, $J = 6.16$ Hz), 8.79 (1H, s), 8.71 (1H, s), 7.89 (2H, s), 7.46 (1H, s), 7.42 (2H, t, $J = 8.24$ Hz), 6.63 (1H, s), 4.27 (2H, d, $J = 6.84$ Hz), 1.32 (3H, t, $J = 6.76$ Hz). ^{13}C NMR (DMSO-d_6, 100 MHz,

δ in ppm) 165.73, 159.33, 153.68, 152.95, 149.95, 148.90, 136.26, 131.26, 123.63, 116.27, 115.01, 113.56, 111.12, 61.86, 14.51. HR-MS: m/z calculated for $C_{20}H_{15}BrN_6O_3S$: 498.0110; found: 499.0115 $[M + H]^+$.

Biological studies

***In vitro* antitubercular activity.** The antitubercular activity of all final molecules (**K1–K26**) was assessed against *Mycobacterium tuberculosis* using the microplate Alamar Blue test (MABA). Resazurin, a thermally stable, non-toxic reagent with cell permeability, is used in this procedure. To prevent test well medium evaporation during incubation, a sterile 96-well microplate with U-shaped wells was filled with 200 μL of sterile deionized water. The synthesized compounds and standard drugs were made in a series of repeated two-fold dilutions (100, 50, 25, 12.5, 6.25, 3.125, 1.6, 0.8, 0.4, and 0.2 μg mL^{-1}) by dissolving them in DMSO. We added 0.2% glycerol and 10% OADC to each well of Middlebrook 7H9 broth, followed by adding 100 μL of *M. tuberculosis* H37Rv (ATCC27294) inoculum to each well. Then, the drugs were introduced to the wells in successive dilutions of ten times. For each plate was wrapped in parafilm, after being incubated for seven days at 37 °C. A freshly made solution of Alamar Blue reagent combined with 10% Tween 80 in a 1 : 1 ratio was added to each well after the initial incubation. After that, the plates were kept in the incubator for 24 h at 37 °C. The wells were shown to change color, with blue denoting bacterial suppression and pink denoting bacterial growth. The lowest concentration of a substance that effectively inhibited bacterial growth was known as the minimum inhibitory concentration (MIC). The reference drugs utilized for comparison were streptomycin (STM) and pyrazinamide (PZA).[26]

***In vitro* bacterial studies.** Using the zone of inhibition assay, all newly synthesized compounds (**K1–K26**) were assessed for their antibacterial efficacy against four bacterial strains, two Gram-positive bacterial strains [*Staphylococcus aurei* (ATCC 23235) and *Bacillus subtilis* (ATCC 6051)] and two Gram-negative bacteria strains [*Pseudomonas aeruginosa* (ATCC 27853) and *Escherichia coli* (ATCC 25922)]. The sterilized nutrient agar medium was divided into two 250-mL conical flasks, each with 100 mL, and allowed to cool to room temperature. Bacterial subcultures grown for 18–24 h were then added to the medium and thoroughly mixed to ensure that the organisms were evenly distributed. The inoculated media was placed evenly into sterilized Petri dishes, with each dish containing approximately 45–50 mL. After the medium had been set, wells were made by punching holes in the agar with a sterile cork borer (6 mm diameter). The test compounds were dissolved in DMSO to provide 100 μg mL^{-1} solutions. 1 mL solution was added to each well and the Petri dishes were incubated at 37 °C for 24–48 h. Following, the growth inhibition zones around each well were measured in millimeters (mm) and compared to those produced by the standard drug.[27]

Cytotoxicity studies

To investigate the new hybrid derivatives' potential in drug testing, cytotoxicity tests were carried out using VERO cell lines. The African green monkey kidney (Catalog number RM10409) was used to generate these cell lines, which were purchased from the National Centre for Cell Sciences (NCCS) in Pune, India. A 96-well flat-bottom microplate was filled with cells, and they underwent incubation overnight at 37 °C, 95% humidity, and 5% CO_2. The cells were then cultured for a further 24 h after being treated with the test samples at different concentrations of 100, 50, 25, 12.5, 6.25, and 3.12 μg mL^{-1}. Following incubation, each well received two PBS washes and 20 μL of MTT staining solution. After that, the plate was incubated for 4 h at 37 °C to enable the cells to metabolize the MTT. Lastly, a microplate reader was used to measure absorbance at 570 nm.

Computational studies

***In silico* ADME studies.** The primary reasons for rejected drug discovery are inadequate pharmacokinetic characteristics, ineffectiveness, and toxicity. The term adsorption, distribution, metabolism, and excretion (ADME) describe a drug's pharmacokinetic characteristics. In other words, these attributes are influenced by the essential chemical aspects of a medication, including its molecular weight, molecular structure, ionization characteristics, and the degree of water solubility and lipophilicity of its various forms.[28] Developing safe and efficient drugs requires an understanding of a drug's ADME properties. Schrodinger's QikProp tool was used to forecast the target compounds' pharmacokinetic characteristics.

***In silico* molecular docking studies.** Molecular docking studies were performed to assess the possible binding interactions of imidazo[1,2-*a*]pyrimidine-thiazole hybrid derivatives (**K1–K26**) with the target enzymes *M. tuberculosis* InhA (PDB ID 1P44) and CYP121 (PDB ID 4KTF). The InhA/CYP121 enzyme was selected for molecular docking investigations because of recent research showing that it has a high affinity for binding to specific pyrimidine and thiazole molecules. Protein structures obtained through the Protein Data Bank (**https://www.rcsb.org/**) were processed with the Protein Preparation Wizard, which included multiple steps such as the removal of heteroatoms and water molecules. GLIDE extra precision (XP) docking was performed utilizing the ligand docking module and an enhanced precision technique. In XP mode, ligand atoms are viewed as flexible, allowing them to change locations and conformations to better interact with the protein's active site.[29] The docking data were evaluated based on docking scores and numerous molecular interactions, including hydrogen bonds and π–π stacking, produced between the imidazo[1,2-*a*]pyrimidine-thiazol hybrids and the amino acid residues within the target proteins' active sites.

DFT studies

Understanding pharmacological molecules' energy characteristics is critical for determining stability, reactivity, and interactions. Drug design relies significantly on studying drug–target interactions, whether they are covalent, ion-dipole, dipole–dipole, hydrogen bonding, or hydrophobic. The ability of density

functional theory (DFT) to reliably predict these interaction intensities is critical for determining its efficacy in computer-aided drug creation. All designed compounds were examined using the Schrodingers Jaguar platform to derive HOMO, LUMO, and MESP. This was accomplished utilizing the B3LYP functional (Lee–Yang–Parr correlation) with the 6-31G++ (d, p) basis set and hybrid DFT, which included Becke, 3-parameter, and Lee–Yang–Parr exchange potential.[30] DFT can calculate key electronic properties that affect drug behavior, including HOMO–LUMO energies, band gap (ΔE), dipole moment, electron affinity (EA), ionization potential (IP), electronegativity (χ), chemical softness (σ), chemical potential (μ), electrophilicity index (ω), and nucleophilicity (N). These characteristics assist in determining molecule reactivity, stability, and potential biological interactions.[31]

Conflicts of interest

Authors declare no conflicts of interest.

Data availability

CCDC 2456909 contains the supplementary crystallographic data for this paper.[32]

The data supporting this article have been included as part of the SI. Crystallographic data for compound **K2** has been deposited at the CCDC/FIZ Karlsruhe deposition service (Deposition Number 2456909 and can be obtained from **https://www.ccdc.cam.ac.uk**. See DOI: **https://doi.org/10.1039/d5ra04692k**.

References

1 S. K. Mishra, G. Tripathi, N. Kishore, R. K. Singh, A. Singh and V. K. Tiwari, *Eur. J. Med. Chem.*, 2017, **137**, 504–544.
2 World Health Organization, *Global Tuberculosis Report*, 2015.
3 A. Koul, E. Arnoult, N. Lounis, J. Guillemont and K. Andries, *Nature*, 2011, **469**, 483–490.
4 V. Singh and K. Chibale, *Acc. Chem. Res.*, 2021, **54**, 2361–2376.
5 P. LoBue, *Curr. Opin. Infect. Dis.*, 2009, **22**, 167–173.
6 A. Sharma, M. De Rosa, N. Singla, G. Singh, R. P. Barnwal and A. Pandey, *J. Med. Chem.*, 2021, **64**, 4359–4395.
7 A. Rasheed, *Med. Med. Sci. Res.*, 2021, **1**, 1–9.
8 A. Que, H. Marrakchi and G. Lane, *Microbiology*, 2000, 289–296.
9 S. D. Joshi, S. R. Dixit, J. Basha, V. H. Kulkarni, T. M. Aminabhavi, M. N. Nadagouda and C. Lherbet, *Bioorg. Chem.*, 2018, **81**, 440–453.
10 S. A. Hudson, K. J. McLean, S. Surade, Y. Yang, D. Leys, A. Ciulli, A. W. Munro and C. Abell, *Angew. Chem., Int. Ed.*, 2012, **51**, 9311–9316.
11 E. Vitaku, D. T. Smith and J. T. Njardarson, *J. Med. Chem.*, 2014, **57**, 10257–10274.
12 V. Finger, M. Kufa, O. Soukup, D. Castagnolo, J. Roh and J. Korabecny, *Eur. J. Med. Chem.*, 2023, **246**, 114946.
13 Y. Teneva, R. Simeonova, V. Valcheva and V. T. Angelova, *Pharmaceuticals*, 2023, **16**(4), 484.
14 H. Doğan, Ş. D. Doğan, M. G. Gündüz, V. S. Krishna, C. Lherbet, D. Sriram, O. Şahin and E. Sarıpınar, *Eur. J. Med. Chem.*, 2020, **188**, 112035.
15 B. Kushwaha, N. Deshwar, M. Priya, B. Chandrasekaran, V. A. Obakachi, R. Chauhan, S. Kidwai, R. Singh, A. Majeed and R. Karpoormath, *J. Mol. Struct.*, 2023, **1276**, 134791.
16 N. M. Panchani and H. S. Joshi, *Russ. J. Org. Chem.*, 2022, **58**, 604–611.
17 R. Reddyrajula and U. K. Dalimba, *New J. Chem.*, 2019, **43**, 16281–16299.
18 S. Roman, I. Sosic, Z. Matej, R. Fernandez-menendez, S. Turk, S. Pajk, D. Alvarez-gomez, E. M. Lopez-roman, C. Gonzales-cortez, J. Rullas-triconado, I. Angulo-barturen, D. Barros, L. Ballell-pages, R. J. Young, L. Encinas and S. Gobec, *J. Med. Chem.*, 2015, **58**, 613–624.
19 M. Hublikar, V. Kadu, J. Kumar, D. Dattatraya, S. Shirame, P. Makam and R. Bhosale, *Arch. Pharm.*, 2020, 1–12.
20 U. B. Karale, V. S. Krishna, E. V. Krishna, A. S. Choudhari, M. Shukla, V. R. Gaikwad, B. Mahizhaveni, S. Chopra, S. Misra, D. Sarkar, D. Sriram, V. N. A. Dusthackeer and H. B. Rode, *Eur. J. Med. Chem.*, 2019, **178**, 315–328.
21 P. Makam, R. Kankanala, A. Prakash and T. Kannan, *Eur. J. Med. Chem.*, 2013, **69**, 564–576.
22 F. Darvas, G. Keseru, A. Papp, G. Dormán, L. Urge and P. Krajcsi, *Curr. Top. Med. Chem.*, 2002, **2**, 1287–1304.
23 M. A. El-Atawy, N. A. Alshaye, N. Elrubi, E. A. Hamed and A. Z. Omar, *Molecules*, 2022, **27**, 4912.
24 N. Nayak, J. Ramprasad and U. Dalimba, *J. Fluor. Chem.*, 2016, **183**, 59–68.
25 M. R. Kuo, H. R. Morbidoni, D. Alland, S. F. Sneddon, B. B. Gourlie, M. M. Staveski, M. Leonard, J. S. Gregory, A. D. Janjigian, C. Yee, J. M. Musser, B. Kreiswirth, H. Iwamoto, R. Perozzo, W. R. Jacobs, J. C. Sacchettini and D. A. Fidock, *J. Biol. Chem.*, 2003, **278**, 20851–20859.
26 J. Vrbanac and R. Slauter, in *A Comprehensive Guide to Toxicology in Nonclinical Drug Development*, Elsevier, 2nd edn, 2017, pp. 39–67.
27 S. B. Rose and R. E. Miller, *J. Bacteriol.*, 1939, **38**, 525–52537.
28 V. Finger, M. Kufa, O. Soukup, D. Castagnolo, J. Roh and J. Korabecny, *Eur. J. Med. Chem.*, 2023, **246**, 114946.
29 S. Khatun, R. P. Bhagat, S. A. Amin, T. Jha and S. Gayen, *Comput. Biol. Med.*, 2024, **175**, 108468.
30 J. Tirado-Rives and W. L. Jorgensen, *J. Chem. Theory Comput.*, 2008, **4**, 297–306.
31 S. LaPointe, D. Weaver and C. Comput, *Aided-Drug Des.*, 2007, **3**, 290–296.
32 D. P, S. Naik, U. D., R. B. C., V. Ranjan and N. S. Veeranagaiah, CCDC 2456909 Experimental Crystal Structure Determination, 2025, DOI: **10.5517/ccdc.csd.cc2ngm4x**.